Improved Power Electronic Converter Topology Using a Variable Inductor for Electric Vehicles

by

Mebrahtom Woldelibanos Beraki

Submitted to the Department of Electrical Engineering, Electronics, Computers and Systems
in partial fulfilment of the requirements for the degree of
Erasmus Mundus Master Course in Sustainable Transportation and Electrical Power Systems
at the
UNIVERSIDAD DE OVIEDO
September 2015

Author . . . . . .
Mebrahtom Woldelibanos Beraki

Certified by. . . . . .
Marina S. Perdigao
Associate Professor
Thesis Supervisor

Certified by. . . . . .
Joao Pedro F. Trovao
Associate Professor
Thesis Supervisor

Certified by. . . . . .
Giulio de Donato
Associate Professor
Thesis Committee

Improved Power Electronic Converter Topology Using a Variable Inductor for Electric Vehicles

by

Mebrahtom Woldelibanos Beraki

Submitted to the Department of Electrical Engineering, Electronics, Computers and Systems

on September 1, 2015, in partial fulfillment of the

requirements for the degree of

Erasmus Mundus Master Course in Sustainable Transportation and Electrical Power Systems

Abstract

The optimal design and implementation of power converters is one of the key aspects in several areas of power electronics application. Nevertheless, the design and implementation of DC-DC converters requires an appropriate buffering via power inductors, the size of which is always a great concern, essentially in electric vehicle (EV) developments.

The design and selection of power inductor plays an essential role in the overall system performance as well as the size of power converter topologies. Therefore, this project is concentrated on the optimal power converter topologies definition based on variable inductor (VI) and focus is given to the design, implementation and testing of bidirectional DC-DC converter and biasing converter for improving the size and efficiency of power converters particularly for sustainable transportation applications.

A particular concern is linked to the implementation of power inductor with a dc-current controlled secondary winding aimed at pre-biasing the core magnetic flux for optimal use

of the magnetic material, in order to reduce the size of the core material, to enhance the current handling capability of power inductors during transient currents, and enable the ripple control in power converters during saturation region operation.

For the implementation of VI, a low-power and low-cost current controlled DC-DC converter is designed and prototype is manufactured to control the secondary winding current in order to adjust the effective inductance of the main winding.

Both the design, modeling, simulation and hardware implementation are addressed. The control of the current controlled DC-DC converter and the half-bridge bidirectional DC-DC converter is implemented in real time program in C2000 launch pad TMS320280273 Piccolo platform.

The experimental results reveal the proposed concept of replacing the conventional power inductors with VI provide superior trade-off in terms miniaturization of power converters, controlling the amount of current ripple and enhancing the saturation level of magnetic cores.

Key words: *Sustainable transportation, bidirectional DC-DC converter, variable inductor, ripple control, electric vehicle, core saturation level*

Thesis Supervisor: Marina S. Perdigao
Title: Associate Professor
Thesis Supervisor: Joao Pedro F. Trovao
Title: Associate Professor

ACRONYMS

CO_2	*Carbon dioxide*
EU	*European Union*
EV	*Electric Vehicle*
PCB	*Printed Circuit Board*
VI	*Variable Inductor*
IGBT	*Insulated Gate Bipolar Transistor*
MOSFET	*Metal-Oxide Semiconductor Field-Effect Transistor*

SYMBOLS

A	*Cross sectional Area (m^2)*
B	*Magnetic flux density (T)*
C	*Buck Converter Capacitance (F)*
$\mathbf{C_{dc}}$	*dc-link capacitor(uF)*
D	*Duty Cycle*
F_{sw}	*Switching Frequency*
H	*Magnetic Field Density (A/m)*
$\mathbf{H_b}$	*Biasing Magnetic Field Density(A/m)*
$\mathbf{i_b}$	*Biasing Current (A)*
$\mathbf{i_{dc}}$	*dc-link Current (A)*
$\mathbf{i_o}$	*Load Current (A)*
$\mathbf{i_s}$	*Source Current (A)*
$\mathbf{i'_s}$	*Modulated Source Current (A)*
$\mathbf{L_b}$	*Control Winding Inductance (mH)*
$\mathbf{L_s}$	*Source Inductance (mH)*
N	*Number of turns*
$\mathbf{N_b}$	*Number of turns in the main winding*
R	*Back converter Load Resistance (Ω)*
$\mathbf{R_b}$	*Biasing Winding Resistance (Ω)*
$\mathbf{V_{dc}}$	*dc-link Voltage (V)*
ω_n	*Undamped natural frequency in (rad/sec)*
ξ	*damping factor*
μ_o	*Permeability of Air (H/m)*
μ_r	*Relative Permeability*
μ	*Permeability of a material(H/m)*
ϕ_b	*Biasing winding flux(Wb)*
ϕ_m	*Main winding flux(Wb)*
$\phi(t)$	*Time changing flux (Wb)*

ACKNOWLEDGMENTS

First of all I would like to thank the Almighty God for his countless blessings and for giving me the will and strength throughout this thesis.

My most sincere gratitude to my supervisors Professor Marina S. Perdigao and Professor Joao Pedro F. Trovao for their diligent guidance, support, encouragement and invaluable mentoring throughout this thesis work. Furthermore, I want to express my gratitude to Professor Giulio de Donato for his willingness to be member of my Master's Thesis committee and for his valuable suggestions.

I would like to express my deep gratitude to Mr. Felipe Machado for all his efforts to make the laboratory run as smooth as possible and the valuable help he provided in solving several problems in the lab. His patience and keen interest to find better and simpler solutions were extremely helpful and inspiring.

I am truly indebted to acknowledge the members of the Electrical Machines laboratory research group at the Institute of Polytechnic Coimbra (ISEC): Professor Paul Pereirinha, Felipe Machado, Nuno Faria and Hugo Neves De Melo for their warm welcome,notable support and creating a comfortable working environment.

I would like to thank to all the members of Department of Electrical Engineering of ISEC particularly the technical and maintenance department Eng. Paulo Queiro, Mr, Fransico Dias and Eng. Sonia Branco for their remarkable support in providing components in need and manufacture of the Printed Circuit Boards.

I would like to express my heartfelt appreciation to my family members and friends for their unconditional love, patience and constant encouragement. My special thanks go to my elder sister Tsige W. Beraki for her boundless care, love and support. Last but not least, my special thanks and appreciation goes to my wife Yordanos and my daughters, Elda, Sidon and Ruth for their patience and understanding throughout my studies.

Mebrahtom W. Beraki

TABLE OF CONTENTS

Chapter Page

LIST OF TABLES

Table Page

LIST OF FIGURES

CHAPTER 1: Introduction

1.1.Problem Definition

The unpredictable nature of fossil fuels, and the global energy challenges of our world require an immediate attention and vital steps are required to combat the greenhouse gas (GHG) emissions. Some of the promising solutions to face these technically demanding challenges are reducing the dependence of fossil fuels by developing innovative alternative technologies, improving the energy efficiency, developing novel technologies in the transportation sector to promote sustainable mobility.

In a global perspective, transportation sector is one of the major contributor of CO_2 emissions. One of the fundamental solutions to address this problem is the development of Electric Vehicles (EVs) and Hybrid Electric Vehicles (HEVs).These technologies have less impact in air and noise pollution, reduce the dependence on fossil fuels, enable regenerative braking and they have better efficiency compared the conventional vehicles [1]. Furthermore, they have worth recording significance in the development of sustainable mobility. Subsequently, there is an immense investment on research and development (R&D) in the areas of energy storage technologies, power electronics, motor drives and charging infrastructure in order to bolster sustainable mobility and reduce ecological damages by reducing GHG emission [1],[2].

Electric vehicles have started since the inception of conventional vehicles, but their development and penetration has been overshadowed by their competitors due to the ease of operation and lower cost of the fossil fuels in the past [3], [4]. In addition, the slow development of electric storage options and the heavy weight of the electrical components used to power up electric vehicles have been some of the main barriers. To address these issues, a lot of research has been done to improve the capacity and types of storage options both at the material and system level, to develop the charging station for electric vehicles and to reduce the size, weight and volume of the power electronic components.

The main objective of this thesis work is based on the latter aspect, and its main focus is to improve the performance of existing bidirectional DC-DC converters. An emphasis is given to the optimization of the bulky power inductors utilized as critical components for buffering bidirectional converters which enable the power flow from energy sources to the load and load to energy sources.

Power inductors are very essential components in power electronic converters and they are built with magnetic materials [5]. Due to the presence of magnetic core, power inductors are bulky components hence they dominate the power stage of power converter topologies. Magnetic materials play a significant role in matching of energy storage systems, filtering, isolation, level shifting, measurement signals sensing, power conditioning and regulation in power electronic converters [6]. Nonetheless, the impact of magnetic materials and magnetics on efficiency, size and density when applied in energy storage and power transformers is very critical.

The need for greater compactness, better manufacturability, and higher performance motivated the adoption of increased switching frequencies [7]. This results in the reduction of power inductors and leads to higher switching losses in power electronic converters. Therefore, it is necessary to find out methods of optimizing power inductors without compromising the size and power losses in power converters.

Generally power inductors are oversized for applications with dynamic load variations, in order to avoid saturation which is a main source of losses and nonlinearity in power inductors [8]. The changing driving cycles in electric vehicles result in abrupt changes in the dynamic loading of EVs. Therefore, it mandates power converter designers for EV applications to be very vigilant when choosing the buffering power inductor. Energy storage devices such as supercapacitors, which have high power and lower energy density are applicable for short durations to store energy during regenerative braking and deliver energy during hard acceleration to meet higher load demands during certain driving cycles. In such circumstances, the peak to peak inductor current could reach very high values much larger than rated and saturation current limit of the power inductor. Therefore, sizing power inductor according to the rated and peak to peak ripple currents,

could lead to the saturation of the magnetic core of the power inductor. Saturation of the magnetic core leads to the reduction of permeability of the core and this in turn causes the decrease of inductance of the power inductor. The inductance reduction results in more current ripples leading to power loss in power converters.

Another option is to size the power inductor to meet the transient peak to peak supercapacitor current levels. However, these currents are much higher than the rated currents, hence this will lead to much larger cores which mandate larger space and weight. In fact, space limitation, efficiency and size are the most critical constraints in traction applications, hence this is not a sound solution to address this challenge.

Considering the above challenges, this thesis work is focused on the optimization of power converter topology, size and efficiency by replacing the bulky saturating power inductors with a multiple winding device, the so-called variable inductor.

1.2.Motivation

The mobility and transport of Europe is heavily dependent on imported oil. In 2013, 94% of the energy consumed in the transportation sector was imported and 84% of these was imported from the politically unstable regions. This puts much pressure in the European Union (EU) economy and trade balance due to price hikes [9].

Therefore, it is very vital for the EU to adopt new policies and strategies to replace oil with alternative fuels and focus on the development of sustainable transportation technologies. These could save the EU 4.2 billion Euros per year in 2020, increasing to 9.3 billion Euros per year in 2030, besides it could result in about 700,000 additional jobs by 2025 [9].

Bearing all the above in mind, the European Union has adopted “20-20-20" Energy and Climate Change strategy, i.e. reducing the CO_2 emissions by 20%, increasing the penetration of renewable by 20% and improving the energy efficiency by 20%, for the 2020,and dedicated commitment to cut CO_2 emissions by 60% in 2050 [10],[11].

Transportation sector is the second largest contributor to the CO_2 emissions in Europe and accounts about a quarter of the total CO_2 emissions. One of the key technologies that could drive this lofty goal is the development of EV and HEV. However, due to the mileage range, slow development of energy storage technologies and the heavy weight of electrical components delayed the growth of these technologies.

With the concept of hybridization of several energy sources, the mileage range is improving. The size and weigh challenge could be ameliorated by optimizing the power electronic components. One of the key power electronic components in EV systems is the DC-DC converter and its size is dominated by the bulky power inductor [12], [13], this is mainly due to the larger size of magnetic cores in order to avoid saturation. This is very critical challenge in applications such as EV and spacecraft electronics where space and lighter weight are critical requirements.

The main motive of this thesis is based on this concept and it is intended to optimize the size, efficiency and reliability of power inductors utilized for traction applications. This concept could be further implemented in other applications such as renewable energy integration, where the introduction of stringent recent grid codes are considered [14], [15].

As this work focuses on the improving the efficiency, size and weight of the power electronic components in EV, it will have a worth recording significance in the consequent accomplishments of the EU and global CO2 emission reduction goals in general and in the transportation sector in particular.

1.3. General Overview

The overall schematic diagram of the system used in this study is depicted in Figure 1. It consists of energy source and storage system, dc-link capacitor, buck-boost bidirectional DC-DC converter for transferring power form energy sources to the load and vice-versa, a dynamic load to emulate an inverter and an electric motor, and a current controlled buck converter (biasing converter) for controlling the current of the control winding in order to monitor the effective inductance of the main winding of the VI during saturation.

The energy source storage system (battery/supercapacitor) supplies power to the dynamic load, and the bidirectional converter acts as a boost converter to step-up the supply voltage to the dc-link voltage during normal operation and hard acceleration, and behaves as step-down converter during regenerative braking to charge the supercapacitor or battery.

The conventional power inductor in power converters is replaced by a VI emulated by two windings as shown in Figure 1. The VI is composed of the main winding, where the main current flows through it, and the secondary winding where a controlled dc current is applied in order to adjust the effective inductance of the main winding during abrupt changes of higher current in the main winding.

The power control layer details are not revealed in Figure 1, they are going to be detailed in other sections. It consists of the dc-link controller, current controller for the bidirectional DC-DC converter and current controller for the current controlled buck converter.

The function of the dc-link controller is to maintain the dc-link voltage at the desired levels so as to provide stable power to the load. The current controller of the bidirectional DC-DC converter monitors the current to be delivered by the energy sources during propelling mode of operation and vice-versa in regenerative mode. Moreover, the controller of the biasing converter is responsible for commanding a controlled dc-current to adjust the level of inductance in the main winding during saturation.

This study is based on the simulation and experimental analysis. Simulations are used to study and validate the designed controllers and the experimental set up is to validate the proposed concept of VI for ripple reduction and core optimization in sustainable transportation.

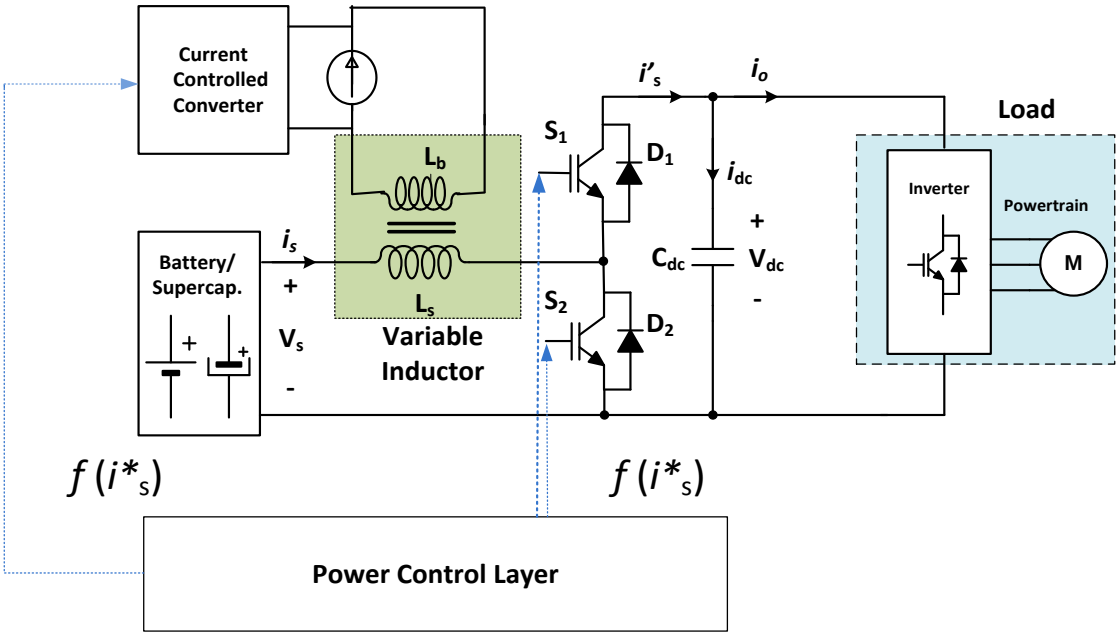

Figure 1: Schematic Diagram of the Study System

1.4. Thesis Outline

This thesis presents the utilization of VI in improving the efficiency, size and volume of power converter topologies for sustainable transportation. It is organized into six chapters.

The first chapter provides a general introduction addressing the problem definition, main motivations of this thesis and the general overview of the overall system.

Chapter 2, provides the detailed literature review on bidirectional DC-DC converters and hybridization of energy sources for EVs. Furthermore, the miniaturization of power inductors, ripple control in DC-DC converters and applications of VI are illustrated.

In chapter 3, the discussion on the variable inductor and the biasing converter are provided. The first part of this chapter focuses on the fundamental concepts of VI and magnetic cores. The details of the biasing converter concentrated on the reasons of selection of the converter, its components selection, mathematical modeling, controller design and implementation and simulation results of the biasing converter are presented

in the second part of chapter 3. Finally, the hardware and software implementation of the biasing converter is illustrated in the last part of the same chapter.

The fourth chapter illustrates the general concepts of bidirectional converters for traction applications, including the specifications of the studied bidirectional DC-DC converter and its average modeling. In addition, the design of the current and voltage controllers are illustrated, and the simulation results are presented at the end of chapter 4.

Chapter 5 deals with the overall system description, experimental set up and experimental results. The brief overview of the system is presented in the first part. Then a brief description of the experimental set up and results are illustrated.

Finally, the main concluding remarks and possible future trends of the work are addressed in the last chapter.

CHAPTER 2: Background and Literature Review

This chapter provides a general overview of the work done in the literature in the following areas: bidirectional DC-DC converters for traction applications, hybridization of energy sources for EVs, miniaturization of power inductors, ripple control in DC-DC converters and an overview of the VI concepts and its application.

2.1. Bidirectional DC-DC Converters for EV Applications

The hybridization of energy sources and storage systems, energy management and the need for matching the battery voltage to the motor rated voltage mandate bidirectional DC- DC converters. These enable reliable operation of energy storage systems, improve the efficiency and reduce EMI emissions from passive components [16].

Bidirectional DC-DC converters are the heart of EVs and they have a remarkable significance in interfacing energy sources and storage systems to the dc-link and manage two way energy transfer in electric vehicles applications.

The conventional unidirectional converters are realized by an active switch, diode and passive components such as inductors, capacitors and resistors. Bidirectional DC-DC converters are derived from the basic DC-DC converters, where the diodes in the unidirectional converters are replaced with active switches either Insulated Gate Bipolar Transistor (IGBT) or Metal-Oxide Semiconductor Field-Effect Transistor (MOSFET) in order to enable bidirectional flow of power [17], [18], [19].

The schematic diagram of bidirectional DC-DC converter and its forward and backward current flow capability in traction applications is revealed in Figure 2. The system is composed of the energy sources, bidirectional DC-DC converter which enable the flow of power in the forward and backward direction, the dc-link, and an electric load. The bidirectional DC-DC Converters in EV power trains enable forward and backward flow of power. In the forward power flow mode, the voltage from the energy storage systems is stepped up by the buck-boost DC-DC Converter to the dc-link voltage level and three phase inverter change the stepped up voltage in to three phase voltage to drive the motor

to create the required torque for acceleration/hill climbing. On the other hand, where, the electric motor works as a generator the regenerated energy flows backwards to recharge the energy sources and the bidirectional converter works as buck converter [20].

Fundamentally, bidirectional DC-DC converters can be grouped into isolated and non-isolated DC-DC converters [21]. Non-isolated converters are used in applications where compact size, higher efficiency, smaller components count and relatively low voltage ratio are required. There are several non-isolated converters which can be used in EV applications both as a unidirectional and bidirectional operations, and the state of the art review of different converter topologies is provided in [22-25]. The cascaded buck-boost, half-bridge, Cuk , Sepic and Split-pi are commonly used DC-DC converters in traction applications [22],[24],[25].

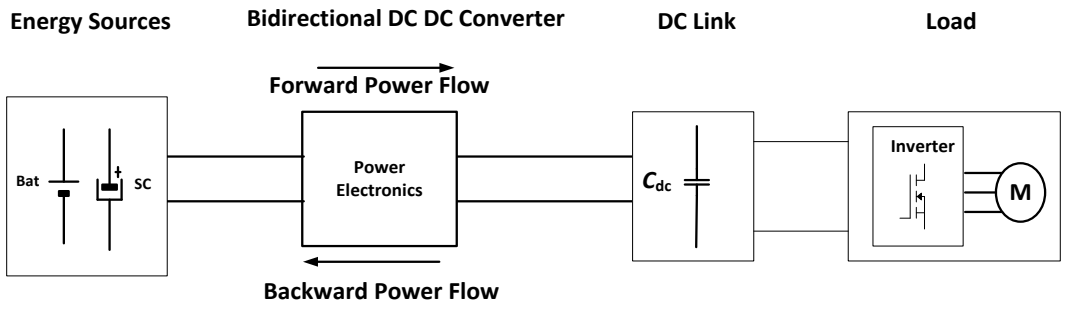

Figure 2: Schematic Illustration of the Study System

However, in applications where there is strict requirement of completely isolating the output from the input and very high conversion ratio, high frequency transformers are used for isolation. Several isolated converters are presented in literature. Half-Bridge, Full-Bridge, Fly-back, Forward and Push-Pull DC-DC converters are some of the commonly used isolated converters which can be used as bidirectional converters [25-27]. The high frequency transformer increases the size, cost, increases EMI , introduces more losses to the system and leads to high voltage stress of the power converter switches [23]. The prominent factor here is the isolation, which is very important in some applications.

Reduced cost, improved efficiency and enhanced overall performance are the key factors for selecting power converters for traction applications [28]. Several DC-DC converters

for electric vehicles applications are compared and their detailed analysis and design is presented in [24]. It is noted that the half-bridge converter has superior performance in terms of efficiency, components count and smaller power inductor but it affects the size of the output capacitor, The simulation and experimental study of several bidirectional converters are presented in [29-31].

To accommodate multiple energy sources and improve the performance efficiency of EVs, multiple input DC-DC converter with a regulated dc-link voltage are required. Consequently reference [32] compared three types of multi input topologies in order to find out optimal design options. The design and sizing of multiple input power electronic converter for electric vehicles propulsion consisting of fuel cell and combined super capacitors and battery units is discussed in reference [33].This paper provides detailed study of the traction drive and driving profile for the proper selection of power electronic components. Furthermore, different topologies of multi-input DC-DC converters are studied, analyzed and their mode of operations are compared, and such converters for power management of power flow in on-board energy sources are discussed in [34-36].

Isolated DC-DC converters with several functionalities such as reducing mismatch of inductor currents and reducing voltage rating of clamping snubber [37], improving the efficiency, [27], Vehicle to Grid (V2G) integration capability, reduced cost and footprint reduction capability [38], and for improving the efficiency and management of energy sources [39] are reported.

The non-isolated bi-directional DC-DC converters for electric vehicles charging performance are compared in [40], accordingly the half-bridge bidirectional dc-dc converter is selected for its prominent significance for electric vehicles applications. High capacity power converter with buck-boost converter topology for optimizing the size and efficiency of components of the power converter is investigated and a prototype is manufactured in [41]. A novel power electronic converter for integrating EV to on-board charger, DC-AC converter and the powertrain is proposed for managing the power flow in different operating modes. This converter has better system efficiency and reliability

and reduces voltage and current ripples and has significant role in the reduction of the size of passive components in comparison to the other topologies [42].

The concept of power electronic converters topologies design, modeling and control is mature area of research. Similarly, a lot of investigations is undertaking on improving the efficiency, size, cost and reliability of power converters for EV applications [42],[43].

Interleaved dc-dc converters have been utilized to achieve these goals [44],[45], however, the interleaving topology requires additional inductors and diodes hence more complexity in control and more components count. Therefore, there is a long way to find out compact, efficient, reliable and simpler DC-DC converters for EV applications. The main goal of this thesis work is focused in achieving this crucial objective in the sustainable vehicular development. The key ideal is focused on the optimization of power inductor size, simultaneously, achieving the smooth bidirectional operation of DC-DC converters and improving the operation and lifespan of storage systems with proper control of the magnetic saturation and current ripples which are the major reasons for the deterioration of energy storage systems. Taking into consideration of the components count the half-bridge bidirectional converter topology is selected for the purpose of this study.

2.2. Hybridization of Energy Storage Sources for EVs

Energy sources and storage are vital components in the commercialization and development of EVs and they have remarkable significance in influencing the performance of electric vehicles [46], [47]. With the present technologies, none of the currently discovered energy sources and storage technologies can fulfill the energy demand of EVs [20], [48], [49]. This is mainly due to the reason that different storage technologies have their own unique features; some of them are applicable for higher power density and others are suitable for higher energy density applications [50].

High energy density sources are reliable for long driving range, whilst high power density sources are applicable for hard acceleration and hill climbing [51]. Hence, the concept of hybridization of several energy sources and storage technologies is very critical and enables optimized utilization of energy sources. On the other hand,

hybridization increases the packaging intricacy, and control of energy sources. Therefore, hybridization of two energy sources with complementary application in terms of energy density and power density are proved to be feasible [49].

Batteries have been used as the main source of power for electric vehicles [47], however, they have lower specific power and energy compared to conventional fuels such as gasoline [51]. Hence, it is very crucial to have more batteries to meet the desired level of performance. However, this increases size, weight and complexity of EVs. Subsequently, researchers both in industry and academia has developed other storage technologies such as supercapacitors in order to couple them with batteries so as to have efficient and reliable hybridization to optimize the size of EV powering infrastructure [4], [49].

On the other hand, sharp dynamic power demands during hard acceleration affect the lifetime of batteries negatively, to surmount this difficulty the hybridization of both batteries and supercapacitors has been introduced and proved to be a reliable combination [52]. Supercapacitors offer higher power density, lifecycle, and efficiency in comparison to batteries. Therefore, the hybridization of both sources create a high power and energy density sources. The emerging high power regenerative braking energy can be absorbed by supercapacitor, and it can be utilized to assist the battery in peak power demands during hard acceleration to enhance battery lifetime, overall system efficiency along with improving the dynamics and reliability of batteries [3-7], [25-27].

Hybridization provides several benefits such as guaranteeing load leveling, assuring regenerative energy recovery, and improving the transient performances [29]. Besides it improves the reliability and lifetime of energy storage systems. It is certain that, this increases the system complexity but provides reliable power source for powering of EVs, improves the efficiency and reliability of EVs. Considering the aforementioned reasons, and the maturity of and cost of battery. It is selected to investigate the feasibility of VI in traction applications.

2.3. Power Inductor Miniaturization for Power Converter Improvement

Power electronic components particularly the power inductor and capacitor have a remarkable significance in the overall performance of EV and influence the size of power electronic converters in various applications. Particularly the power inductor has a significant contribution on the size and weight of the power electronic converters utilized in EVs mainly due to the core material limitation, core materials losses and their impact in the transient performance of the overall system [53].

The inevitable need for lighter, compact and efficient power converters motivates the pursuit of R& D to develop miniaturized power electronic converters with a key focus of enhancing the saturation level and reducing the size of magnetic cores, and improving the efficiency [54]. To achieve the objective of optimizing the magnetic cores and obtain lighter power inductors for DC-DC converters, several methods such as the development of new materials, winding structures, assembly techniques, insertion of permanent magnet in the air gap and increasing the switching frequency have been proposed and investigated in [6],[7], [53]. Furthermore, in order to improve the size and efficiency of power electronic converters in EV [55],[56], proposed integrated winding coupled inductor to reduce the volume, weight and cost of magnetic components by the number of turns and cross sectional area of the magnetic core for efficient power conversion. This configuration uses coupled inductors and auxiliary coils and has two switches and diodes, hence more components count compared the VI considered in this study. Besides, the close coupling of the inductors results in heat and causes stray capacitance which results in the increase of switching losses [56].

Interleaved coupled inductor based boost dc-dc converters for interfacing several energy storage systems such as fuel cells, batteries and supercapacitors for achieving higher efficiency with reduced size of output filter is discussed in [57]. This converter provides improved efficiency compared to the conventional boost converter but it faces higher voltage stress and requires additional clamping components. Bearing all this in mind, this study focuses on the VI concept to replace the bulky power inductors for improved efficiency, ripple control and magnetic core optimization.

2.4.Ripple control of DC-DC Converters

In traction applications, the operation of the bidirectional converter results in current ripples due to the switching of the alternate switches in the power converter. The ripple current is one of the main aspects which influence the operation, lifespan and efficiency in power electronic converters based energy storage systems and the energy source systems [45],[58-61]. Particularly, in battery powered EVs, the ripple current influences the electrochemical characteristics and degrade their performance in actual driving cycles [61]. Hence several power converter topologies have been developed with the main purpose of reducing the current ripple in order to improve the efficiency, reduce the size, improve the transient response and improve reliability [60], [62], [63].

The use of multi-phases with interleaving technique and connecting capacitors in parallel to energy storage systems are commonly used for reducing the current ripple in DC-DC converters [60], [64].Coupled inductor interleaved converters are among the most popular topologies for reducing the ripple content of current in DC-DC converters for EV and reduction of the size and the weight of passive components [13]. These converters have worth recording significance in improving the electrical performance, size ,weight, reducing the winding loss, and reducing the input and inductor ripple current and dc flux cancelation [65]. Nevertheless, their performance depends on very precise coupling within the magnetic circuit, small variations in the coupling affect the ripple variation [66]. Furthermore, the leakage inductance of the coupled inductor results in high voltage spikes which increases the switching stress resulting in serious EMI noise and affects the charging and discharging of energy storage systems [22], [67].

For extending the battery life and enabling portable devices to operate under light load conditions and to regulate the current ripple adaptively programmable hysteresis control scheme is proposed in [68].Besides, the proposed control scheme improves the efficiency of the DC-DC converter by reducing the conduction and switching losses in a battery powered applications. However, its application is for low power applications and the switching frequency depends on the operating conditions, hence it could increase the losses in the output filter [69]. Active power filtering method using the decomposition of

the dc-bus current is utilized to minimize the ripple content of current for batteries [61]. But this method is based on the approximations from the motor and inverter parameters and require powerful controllers which makes is complex. Multi sampled digitally controlled dc-dc converter with switching ripple compensation is discussed in [70].This control scheme requires higher clock cycles hence it is very difficult to implement in smaller microcontrollers. In reference [71] sliding mode control based on neural networks is utilized for ripple control of fuel cell for clean energy generation, it offers higher performance at lower cost.

Adaptive frequency control, where the switching frequency is changed as a function of current with the decrease of inductance is investigated in [72]. However, to achieve this, higher switching frequency is required, which in turn will lead to the increase in the switching losses. Coupling inductor to a self-lift Sepic converter based boost converter is used for reducing the ripple current and enhances the power density in fuel cells applications [73]. This solution is promising but its complexity makes it not effective for EVs.

Active filtering which replaces larger passive components with smaller passive components for improving the common mode inductor performance is described in [74]. Controlling the current ripple assures the reduction of passive filters components size, weight, volume and cost of power converters. The aforementioned ripple control techniques provide a significant improvement in ripple control, but due to the components count and complexity of control, they are not effective for EV applications as compactness and lighter weight of components are key requirements. Therefore, it is very crucial to find better methods of ripple control for DC-DC converters for EV applications.

2.5. VI and its Applications

Power inductors are dynamic energy storage devices which are present in several power electronics converters and provide energy storage in various operation modes of electronic circuits. Furthermore they have remarkable significance as filters in power electronic converters, resonant circuits and rate of current change limiters in snubber

circuits [75]. Power inductors are very crucial in attenuating ripple, electromagnetic interface (EMI) and improving the power quality [76].

Inductors can be categorized as saturating or VIs. In case of saturating inductors the increase of current leads to the decrease of the effective inductance due to the decrease of the relative permeability (which in turn increases the reluctance of magnetic cores). Therefore, they are applicable for applications where there is no much variation of the current and their efficiency and performance is degraded if operated above the saturation current However, in case of VI the value of inductance can be varied as response to a control current according to the desired value [77], [78].

Applications which require dynamic loading and unpredictable driving cycle patterns are constrained by saturating inductances. Servo systems have been used to mechanically vary the inductance of power inductors which is very demanding and not efficient [79]. A VI which is composed of a main winding and a control winding enables the variation of inductance electrically. In the proposed application, the control winding is utilized to adjust the effective inductance of the main winding in operations above the saturation level of the power inductor. These VIs can provide robust, efficient and reliable performance for applications where there is dynamic load variation [77], [78].

VIs have been effective in applications which require considerable variations in current such as PV systems [80], [81], electric lighting systems [82],[83] VAR compensation in electrical power system networks [84], air craft industry [85] and electric vehicles [53] Furthermore, they have worth recording applications in resonant DC-DC converters [86], power factor correction [83], harmonic control and voltage regulations [78].

VIs have been realized by moving air gap [78], moving core, switched inductance decade boxes, gyrator circuitry [85], two winding coils [53],[85],[87], [82] and permanent magnets [12].

Several core configurations for the realization of VI are presented in literature. The most commonly used structures are gapped double E cores. Also, toroidal cores with an air gap and two windings placed in the same core, two toroidal cores, where the main winding is

placed in the center and the control winding on the sides of the two cores, - -, pot cores, C cores, orthogonal cores and so forth depending on the application [83], [87],[88],[89],[90],[91].

The practical design of double E core structure of VI for high-frequency application of resonant AC-DC and DC-DC converters is detailed in [90]. The application of VI in the regulation and control of DC-DC converters for photovoltaic energy harvesting is illustrated in [81].The utilization of VI provides significant inductor volume reduction and considerable improvement in the performance of MPPT control algorithm in PV systems.

The comparison of different techniques for VIs implementation and the fundamental mathematical equations which characterize a VI are provided in [85]. In [92] a method of predicting the inductance of a coil with change of an applied DC current is proposed for optimization of the power inductor for power conversion applications. The large signal characterization of VI along with its remarkable ripple and volume reduction potential in traction applications is discussed [53].The 3D finite element analysis model of VI is studied in [79] and used to model distribution of flux density and determine the region of saturation. The detailed modeling and behavioral model of VI for magnetically controlled electronic ballasts with E core magnetic material is presented in [87].

Due to the various terrains in practical applications of EVs, there are transient currents which could result in the saturation of the magnetic material. Magnetic saturation is one of the key properties which impact the selection of power inductors. The value of power inductor is heavily dependent on the amount of current flowing across it. Large currents require large volume and size inductor cores, if smaller ones are used the magnetic material will saturate and as consequence the value of the power inductance will be reduced leading to more ripple and losses. This constraint can be addressed by having larger core inductors which in fact is not suitable for traction applications, where space and weight are key constraints.

Another solution to this challenge is the utilization of VI, where the inductance value is adjusted with the control winding depending on the current levels of the main winding. The DC biasing has been proved to be applicable for this application. By controlling the current in the control winding, the saturation level of power inductors can be enhanced [85]. This concept enables the reduction of the size and weight of power electronic converters in EVs, by reducing the size of bulky power inductor.

CHAPTER 3: Variable Inductor and Biasing Converter

3.1. Variable Inductor Fundamental Concepts

A VI is a dc-current controlled, multiple winding inductor realized in various geometries and magnetic cores [53]. It consists of a main winding and the a control winding where the dc-control current is applied in order to adjust the inductance of the main winding. The controlled current in the control winding is used to alter the magnetic property of the main winding and adjust the operating point of the core in the B-H saturation curve [85].

To clearly understand the concept of VI it is necessary to revisit the basic concepts of electromagnetism.

The fundamental notion of Faraday's law of electromagnetic induction is that a changing magnetic flux crossing a conductor induces an electromotive force. Mathematically,

$$v(t) = \frac{Nd\phi(t)}{dt} \tag{1}$$

Where $v(t)$ is the induced voltage, N is the number of turns and $\phi(t)$ is the time changing flux across a conductor.

In magnetic materials, the flux density and magnetic field are related as shown in the following equation:

$$B = \mu H \tag{2}$$

Where B is the magnetic flux density, H is the magnetic field and μ is the permeability of the magnetic material.

For a given flux (ϕ), and current (I) the inductance is the ratio of flux to the current across an inductor. Mathematically,

$$L = \frac{\phi}{I} \tag{3}$$

Rewriting the flux in terms of the physical parameters of the core material and the magnetomotive force, the inductance of a given material can be expressed as [85]:

$$L = \frac{N^2 \mu A}{l} \tag{4}$$

Where N the number of is turns, A is the cross sectional area of the core material, l is mean length core material and μ is the permeability of the magnetic material, which is the product of the relative permeability of a material and the permeability of vacuum (air).

The inductance of material depends up on several variables. To vary the inductance, it is required to change any one of the four variables revealed in equation (4).The number of turns (N), the area (A) and the mean length (l) are fundamentally dependent on the geometry of the core material. To change any one of the three variables we need to change and move the physical structures which is very cumbersome and not effective. However, the permeability of a magnetic core is the characteristic that gives the core an ability to concentrate lines of magnetic flux and it can be modified in an easier way. Consequently, this property of magnetic cores is exploited to realize the VI by changing the effective permeability of a magnetic core which is dependent on the core material property rather than the physical structure. This technique is demonstrated throughout this work for traction applications.

Revisiting equation (4), the inductance as a function of current can be expressed as:

$$L(i) = \frac{\mu_r(i) \mu_o A_c N^2}{l} \tag{5}$$

Where $\mu_o = 4\pi \times 10^{-7}\ \mathrm{H \cdot m^{-1}}$, $\mu_r(i)$ is the relative permeability as a function of current and $L(i)$ is the inductance as a function of current.

The control winding magnetic field can be determined from the control current and the control winding number of turns as shown below.

$$H_b = \frac{N_b i_b}{l} \tag{6}$$

Where N_b is the control winding number of turns and i_b is the control current required to adjust the permeability of the core, in order to enhance the saturation level of the magnetic core.

The above equations are used to characterize and understand the principle of VI concepts. From the above equations it can be clearly observed that the inductance of a magnetic material depends up on the permeability of the magnetic core and it in turn depends up on the magnetomotive force (mmf).Hence, by changing the mmf either by adding to or subtracting from the main winding mmf, the permeability of the control winding is modified, hence it can be used to adjust the effective inductance of the main power inductor. The control winding should provide very low current. Therefore, it should be designed with a high number of turns of smaller cross sectional area wires. Since a DC electrical signal is going to be used to adjust the value of the main winding inductance, the number of turns for the biasing winding is best determined through numerical solution or experimentation [85].

The variable inductor under study is s realized by two sets of windings, the main winding and the control winding. Both windings are wound in the same core in such a way that there is no magnetic coupling between them. The main winding is connected to the main supply and the control winding is connected to the current controlled DC-DC converter. The dc-current is used to adjust and monitor the inductance of the main winding by changing the permeability of the core [66].

3.2.Magnetic Cores and Parameters of the VI Prototype

As previously mentioned, in power inductors the magnetic core plays very significant role in increasing and concentrating magnetic fields. On the other hand, the magnetic core of an inductor introduces core losses and it limits the maximum current handling capability of power inductors and this is constrained by the material's B-H

characterization curve. Therefore, the choice of core materials and geometrical shapes are fundamental design considerations.

In the present days there are ample magnetic cores options such as ferrite cores, permalloy powder cores, Kool Mμ®powder cores, 50 Ni/50 Fe powder cores, tape wound cores, cut cores, bobbin cores, laminations and powdered iron cores are some magnetic cores that can be used for several applications [93]. Ferrite cores and powdered iron cores are the most commonly used for inductors in power converters.

Powdered iron cores have distributed air gap structure, soft saturation and dc bias characteristics which makes them suitable for power converters due to their smaller core sizes, ease of winding and they have better saturation characteristics. Besides, they are available in range of shapes, sizes and permeability [93],[94]. On the other hand, ferrite cores have discrete air gap which makes them suitable for high-frequency with low core loss applications. Alike the powdered iron cores, they have also dc bias characteristic [93].

Selecting an appropriate power inductor for specific application requires several aspects such as energy storage requirement, space, cost, EMI and winding flexibility [95]. Bearing all these in mind, Toroidal ferrite cores are used for their low core loss, cost, their potential to offer smaller volume and well contained magnetic flux density, hence relatively smaller EMI [96].

The VI is composed of two cores each of them are made by stacking two cores (this was done due to availability constraints of core, the two cores are used to avoid the quick saturation of the magnetic core and enable higher levels of current). Using two stacked cores in each side of the VI introduced a parasitic capacitance that in turn created undesired resonant oscillations and affected the current and voltage waveforms of the VI under normal operation. In a future optimized solution, the oscillations that will be present in the experimental results can be removed. The VI prototype built with Toroidal ferrite cores in [53] is used as prototype for testing the biasing converter and realization

of bidirectional converter in order to investigate its potential significance in sustainable transportation applications.

Figure 3 depicts the schematic diagram of the VI prototype which is composed of two toroidal cores, the main winding and control winding, and the biasing converter. Both the main winding and the control winding number of turns are equally divided into the two Toroidal cores. The control winding coils are wound in such a way to cancel out the transformer action effect of the two windings. The directions of flux are shown where red is for flux in the control winding and the blue one is the direction of magnetic flux in the main winding.

The current controlled converter is a low power, small buck converter designed to provide small current to the control winding. This converter is ultimately responsible for adjusting the effective inductance of the main winding, to reduce the effect of saturation, by providing a regulated dc current.

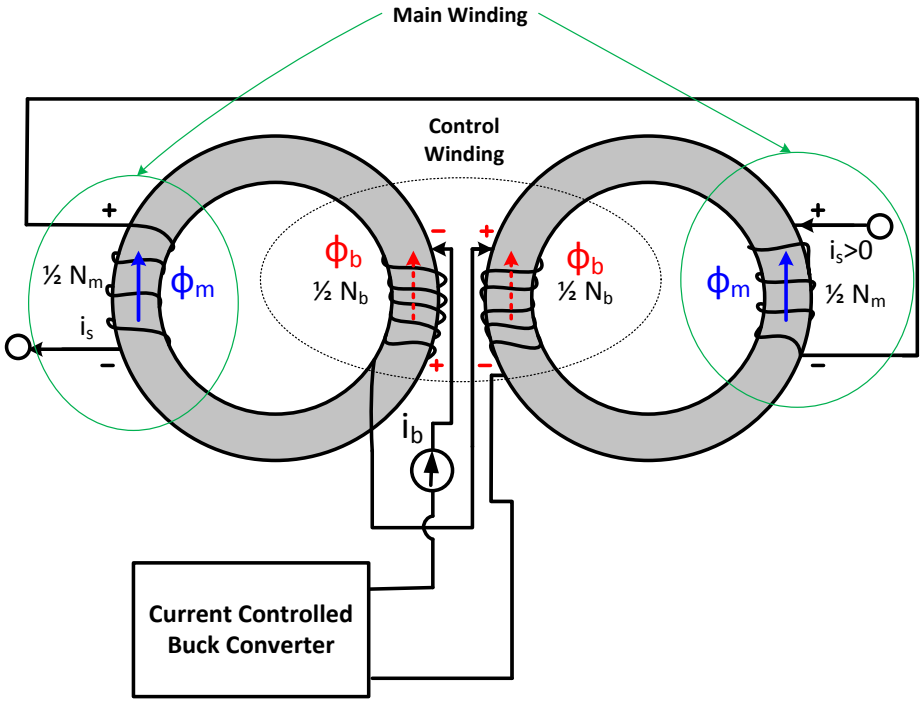

Figure 3: Schematic diagram of VI Prototype with its Control Converter

The specifications the power inductor prototype are detailed in Table 1. As it can be clearly shown, the biasing winding number of turns is much higher than the main winding. However, the main winding is made up of about 6.5 times larger wire gauge.

Table 1.Toroidal Core Dimensions and VI Parameters

Ferrite core Toroid R 102 × 65.8 × 15.0 (mm) with Epoxy coating		
Core Volume:	0.068 dm3	Core Material: N87
Core Diameter (external)	102 mm	from EPCOS
Core Diameter (internal)	65 mm	
Core Height	15 mm	
VI prototype		
Power Inductor Wire Gage:	4.17 mm2	
Bias Winding Wire Gage:	0.65 mm2	
Number of turns in the main winding ($\mathbf{N_m}$)	28	
Number of turns in the bias winding ($\mathbf{N_b}$)	360	
Total VI Core Volume:	0.273 dm3	

3.3.Biasing Converter

3.3.1 Biasing Converter Selection

One of the main of objectives of this project is to optimize the size and performance of power converters for EV applications based on the utilization of a controllable power inductor. In order to have a small size solution, the biasing converter should be as compact as possible so as its contribution to the overall dimension and volume the proposed power inductor (or VI) is not significant.

The step-down family of DC-DC converters are suitable for this application. The filter at the output of these converters can provide a controlled current if operating in continuous current mode (CCM).The possible converter topologies which could be suitable for this specific application are the buck, forward, push-pull and full-bridge DC-DC converters [97]. All these converters can work as a current source. The forward converter provides isolation and can act as current source and it is preferable when high output currents are required. However, it is composed of transformer, diodes, and tertiary coil, which increases the size, the components count and increase the power losses. Therefore, the efficiency is lower. Similarly, the push-pull and half-bridge and full-bridge converters are not suitable, due to their components count and lower efficiency. Therefore, taking into consideration of the number of components, areas of application and efficiency, and ease

of implementation and simplicity, the buck converter is selected as a biasing circuit of the variable inductor.

3.3.2 Biasing Converter Components Selection

The main design parameters for DC-DC converters are the input voltage range, the output voltage range, the maximum output current (current ripple), the voltage ripple and the switching frequency. These parameters are very important for the sizing and selection of components in DC-DC converters. The design specifications of the required converter are shown in Table 3. Accordingly, the converter components are selected using the design procedures presented in [97].

An inductor and capacitor are critical components in DC-DC converters, hence their selection requires meticulous attention. When selecting the inductor CCM is assumed and the ripple current is made very small, so as not to have an effect on the main power inductor. In the same manner, the output capacitor is selected to minimize the voltage ripple and overshoot.

Table 2 Buck Converter Design Specifications

	Symbol	Value	Unit
Nominal Input Voltage	Vin	12	V
Nominal output voltage	Vo	3	V
Current ripple	ΔI	5%	
Voltage ripple	ΔV	10%	
PWM switching frequency	F_{sw}	20	kHz

The selected power converter with its components is shown in Figure 4. MOSFET is selected as a switching device and the inductor and capacitor are estimated using the classical design procedures. In the actual implementation, the load is replaced by the biasing winding and the current to the winding is controlled through the value of the duty-cycle. In later obtained experimental results it is possible to observe that the ripple level of the control current is not as low as expected.

3.3.3 Mathematical Modeling of Buck Converter

The schematic diagram of the buck converter and its average model are depicted in Figure 4 (a) and (b) respectively. When the switch is on, the inductor stores energy and the stored energy is exchanged between the capacitor, inductor and load, when the switch is in the off state.

The dynamic average model of the buck converter can be obtained from the simplified average model of the buck converter is shown Figure 4 (b) . The set of equations for the reduced average model of the buck converter can be written as:

$$L\frac{di_L(t)}{dt} = dV_{in} - V_c(t) \tag{7}$$

$$C\frac{dv_C(t)}{dt} = i_L(t) - \frac{v_c(t)}{R} \tag{8}$$

Replacing i_L from equation (7) into equation (8) the dynamic model of the buck converter is reduced in to (9):

$$dV_{in} = CL\frac{d^2v_c(t)}{dt^2} + \frac{L}{R}\frac{dv_c(t)}{dt} + v_c \tag{9}$$

Replacing $v_c = i_b R$ and taking the Laplace transform of the output-current to the control transfer function will be reduced as shown in equation (10).

$$\frac{i_b(s)}{d(s)} = \frac{V_{in}}{RLCs^2 + Ls + R} \tag{10}$$

When the load is replaced by the control winding circuit, which consists of an inductance and a series resistance, the above model will be changed into a more complex system as shown below.

$$\frac{i_b(s)}{d(s)} = \frac{V_{in}}{LL_bCs^3 + LCR_bs^2 + (L + L_b)s + R_b} \tag{11}$$

The dynamic model of the converter and the dynamic load is third order system, however, the third pole is very far from the dominant poles hence the system can be reduced to second order system.

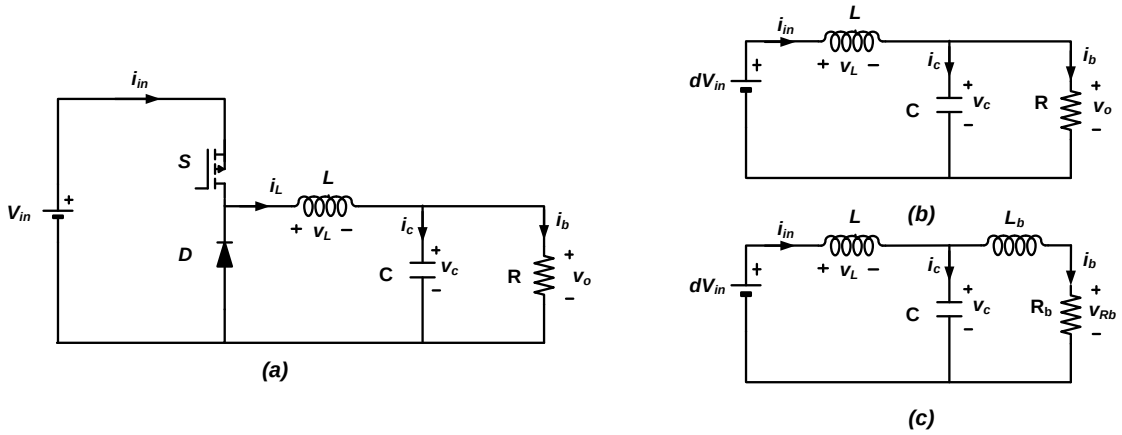

Figure 4: (a) Schematic diagram of buck converter (b) Simplified average model of buck converter with Resistive load (c) Simplified average model of buck converter with control winding as load

The characteristics of the designed buck converter is highly influenced by the control winding. This is verified from the fundamental step response of both the third order and first order plants. The third order system obtained from all the parameters of the converter can be reduced to first order system with transfer function of the control winding. The step response is presented in Figure 5. It can be shown that the third order model of the system can be approximated by the first order system.

It can be observed that the system response is slow due to the high inductance of the control winding. The zoomed image shows that both systems have the same transient response with slight variations in the third order system. The slight variation is introduced due to the buck converter parameters. Nonetheless, these variations are insignificant therefore they can be neglected for the analysis and control design of the system.

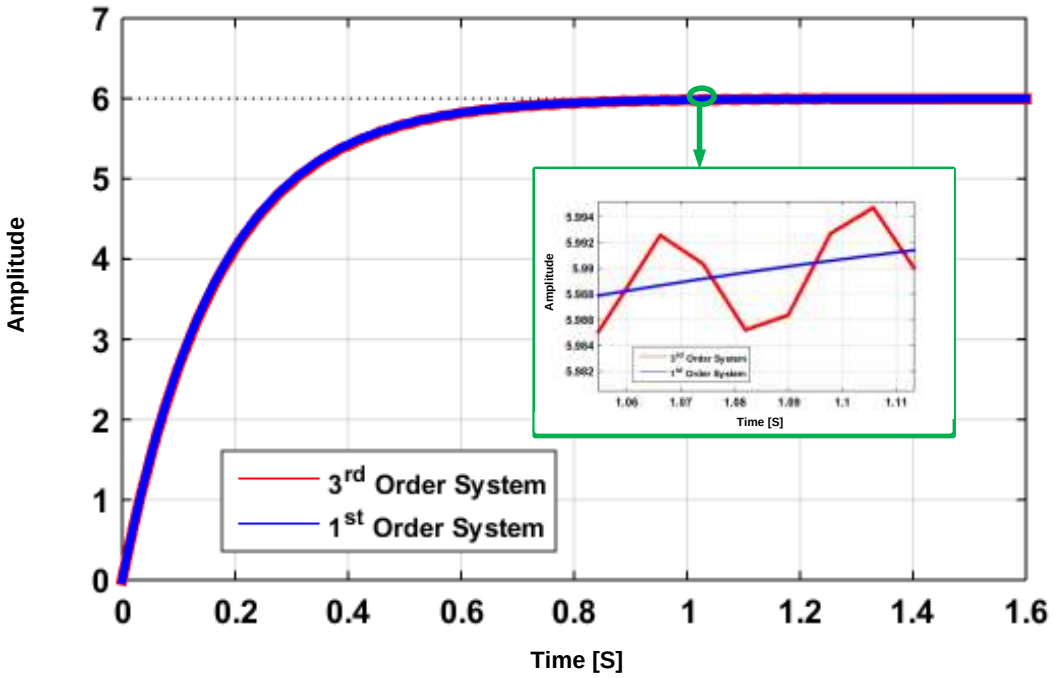

Figure 5: Step Response of both the third order system and the first order system

3.3.4 Controller Design and Digital Implementation

The mathematical modeling of the buck converter is illustrated in the previous section. To achieve the control of the switching of the buck converter and enable the commanding of the required current to the control winding of the VI, the conventional Proportional Integral (PI) controller is chosen.

The general transfer function of a PI controller is given as:

$$C(s) = \frac{K_p s + K_i}{s} \tag{12}$$

Where K_p and K_i are the proportional gain and integral gain in respective order. These gain parameters are determined analytically using the procedures utilized in [98-100].

Revisiting the transfer function which related the current across the control winding both as a function of the input parameters and circuit parameters which is expressed in equation (11) and ignoring the buck converter parameters due to the reasons discussed above, the control parameters can be calculated,

The closed loop transfer function of both the current controller and the transfer function of the control winding plant can be written as:

$$\frac{i_b(s)}{i^*_b(s)} = \frac{\frac{K_p{}^b}{L_b}(s + \frac{K_i{}^b}{K_p{}^b})}{s^2 + \frac{(R_b + K_p{}^b)}{L_b}s + \frac{K_i{}^b}{L_b}} \tag{13}$$

Where $K_p{}^b$ and $K_i{}^b$ are the proportional and integral gain of the control winding current controller respectively. The superscript * is to indicate a reference value (set value) of a signal.

Furthermore, the general second order transfer function of a dynamic system is expressed as in (14).

$$G_{so}(s) = \frac{\omega_n{}^2(\frac{s}{z} + 1)}{s^2 + 2\omega_n\xi s + \omega^2} \tag{14}$$

Where ω_n is the undammed natural frequency which indicates the speed of the response, ξ is the damping factor which determines the shape of the response and the amount of oscillations and z is the zero which affects the transient performance of the system in terms of overshoot, undershoot and transient performance parameters but it does have no effect on the stability of the system. The design specifications ξ and ω_n are chosen based on the desired settling time and output overshoot.

In this work, the controller is designed based on ξ chosen 0.707 and ω_n is selected to be 1/20 times the switching frequency in (rad/s) to meet the desired design specifications, taking into consideration the specifications of the other controllers.

By comparing the denominators of equations (13) and (14), the gain parameters of the controller are determined as in (15) and (16).The superscript b is used to indicate these gains are the gains of the biasing converter current controller.

$$K_p{}^b = 2 \times \omega_n \times \xi \times L_b - R_b \tag{7}$$

$$K_i^{\,b} = \omega_n^{\,2} \times L_b \tag{8}$$

The schematic diagram of the controller of the current controlled buck converter is revealed in Figure 6. It consists of the reference current calculator which senses the main winding current and compares the main wining current with the saturation level of the main winding. When the main winding current is within the limit of the saturation level, the control current estimator sets the reference current of the control winding zero, therefore the buck converter is idle in normal operation. However, in situations where, the main winding current is higher than the saturation level of the main winding, the current calculator block estimates the reference current for the biasing converter. In open loop studies of the system, the reference current of the buck converter is set manually. However, in the closed loop operation of the system, the control current is determined from the main winding current levels.

Following the estimation of control current reference, the current across the biasing winding is sensed and it is compared with the reference current. Subsequently, the error signal is obtained and accordingly the controller process the error signal to obtain the control command. The control command is modulated with triangular carrier signal at higher frequency to generate PWM signals to control the switching of the current controlled converter. This converter provides precisely controlled current to the control winding and with this controlled current the control winding produces dc mmf to cancel out the dc flux created in the main winding to enhance the saturation level of the magnetic core.

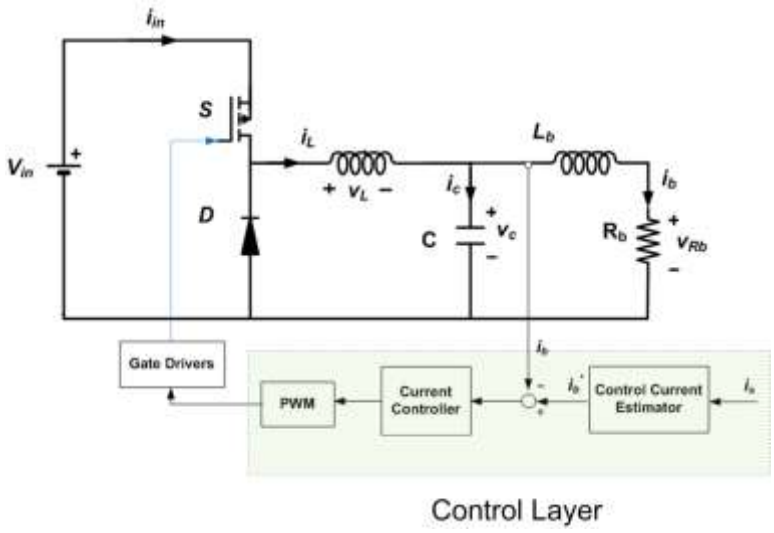

Figure 6: Schematic diagram the buck converter and its control

For practical implementation of the controller in TMS320F28027 Piccolo Microcontroller, digital conversion is required. Different methods are used for converting continuous domain controllers to digital domain. Tustin approximation is the most commonly used since it allows minimal sharp changes in the integral action during sudden changes in the reference and measured signals. Hence this method is selected for this thesis. To convert the controller into digital domain, the Laplace operator s is replaced the following the expression:

$$s = \frac{2}{T_s}\left(\frac{z_d - 1}{z_d + 1}\right) \tag{9}$$

Where T_s is the sampling time and z_d is the digital representation operator in the z plane.

The digital domain is used for practical implementation of the controller and the analog one is used for simulation purposes.

3.3.5 Biasing Converter Simulation Results

The functionality of the biasing converter and its controller are evaluated through simulations prior to the practical implementation of the converter. Figure 7 reveals the simulation of the buck converter connected to the biasing winding. An input supply

voltage of 12V is applied and the reference current is set as different step signals to validate the functionality of the controller and its robustness for various changes of current. From these reference currents, the transient and steady state performance of the controller are investigated.

As the biasing converter is designed to be small, its operating current can reach up to 1.5A.Therefore, the step reference current is selected to be in this range. At t=0, the current reference is changed from 0A to 0.5A. At the beginning, the controller response is slow, as shown in the graph, but it is within the limit of the settling time specification. In steady-state both reference current and measured current match each other. In the next interval from t=0.5 seconds, the reference current is stepped up from 0.5A to 0.8A and increased further to 1A in the next interval. In steady state both the reference and measured signal align to each other but the transient response is the same as the previous case. At t=1.5 seconds, the current reference is stepped down from 1A to 0.8A. During this time, the performance of the controller is much slower than in the previous situations. This is mainly due to the inductance of the control winding, as this winding has large inductance values, it does not allow a sudden fall of current, and hence the transient response is very slow during this time. The transient response is revealed in the zoomed signal. In the next interval, the current reference is increased to 1.2A in two steps and the transient response is the same as in the first three intervals.

As a representative of the increasing current reference injection, a zoomed version of the transient response is revealed at t=2.5 seconds. It can be shown that the measured current tracks it reference value with a settling time of less than 10ms. From these simulations, it can be observed that the reference current and the measured current align each other which reveals satisfactory current control. Varying step currents are simulated in order to test the robustness of the controller.

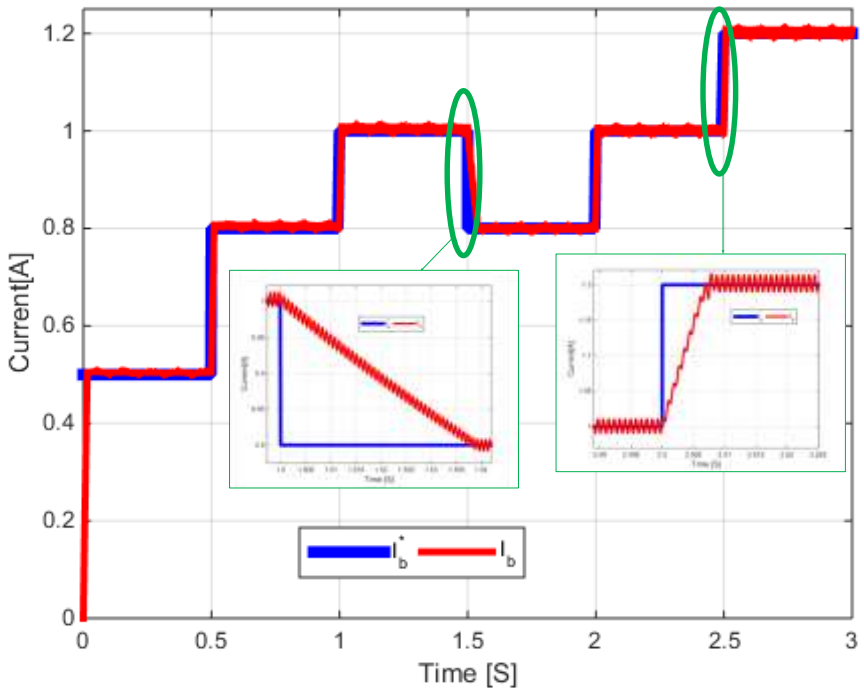

Figure 7: Current Controlled DC-DC Converter Currents

3.4.Implementation of the Biasing Converter and its Control

The main purpose of the biasing circuit is to adaptively control the inductance of the main winding to reduce the saturation effect by providing controlled current to the control winding. To achieve this objective low-cost and low-power current controlled buck converter is proposed, designed and implemented.

3.4.1 Hardware Implementation of the Biasing Circuit and its Control

In order to have a compact converter, the buck converter is implemented in printed circuit board (PCB). The PCB is composed of the proposed converter with all its components, its driver circuit, current sensor, filter components, power supply connectors and interfacing circuits, and it is designed in *Altium Designer Software*. The PCB of the converter is designed with two ground planes in order to reduce the noise and capacitance between different ground points. All the grounds in the sensor circuit are connected to one ground plane and all the ground points in the power circuit are connected to second ground plane and finally the two ground planes are connected to the same point.

The buck converter circuit is composed of the main components and the MOSFET Driver circuit. The interfacing circuit is composed of the current sensor and its scaling circuit. The interfacing circuit is not functioning due a problem in the scaling circuit. The top layer and bottom layer of the manufactured PCB are revealed in Figure 8 (a) and (b) respectively. It can be noted from the diagram the PCB has two ground planes, one for the power circuit and another one for the scaling circuit and both ground planes are connected at one point.

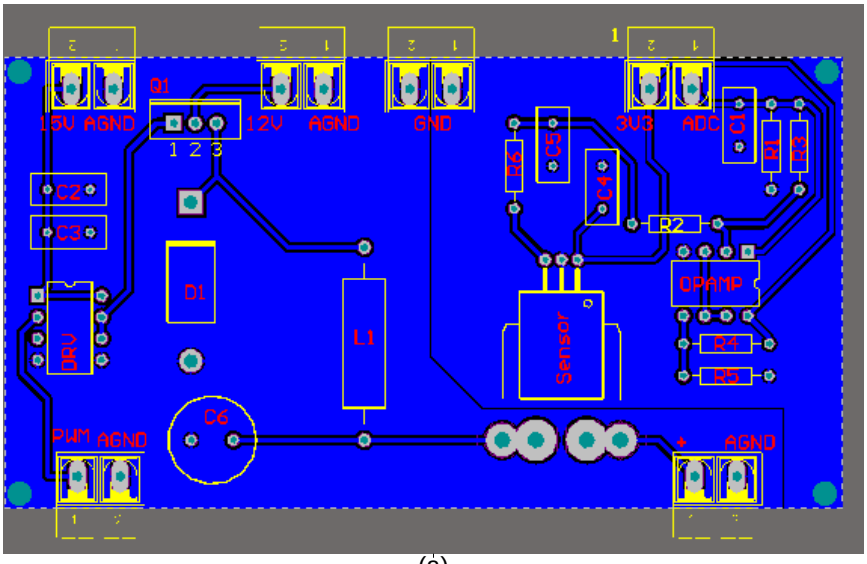

(a)

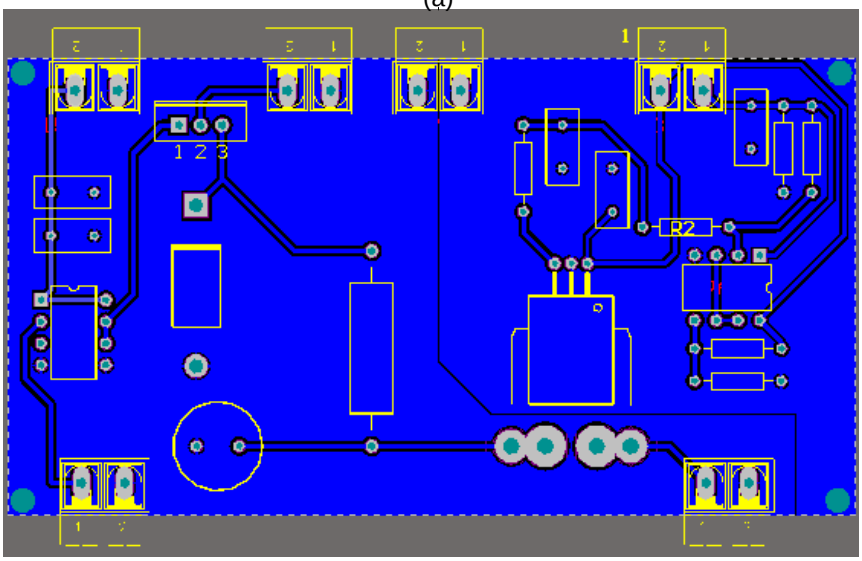

(b)

Figure 8:PCB of Buck Converter (a) Top Layer (b) Bottom Layer

The buck converter is designed to operate for small currents, therefore to solve the problem faced in the interfacing circuit, very small INA193AIDBVT precision current sensor and the LM4132AMF-2.0/NOPB voltage regulator are implemented to provide precise measurements. The schematic diagram of the modified system including the precision current sensor and the voltage regulator is shown in Figure 9.

The control algorithm is developed in real time program in The C2000™ Piccolo™ LaunchPad™-F28027 low-cost experimenter board. The schematic diagram of the hardware implementation of the biasing converter is revealed in Figure 9.The precision current sensor is power from the piccolo 3.3V.

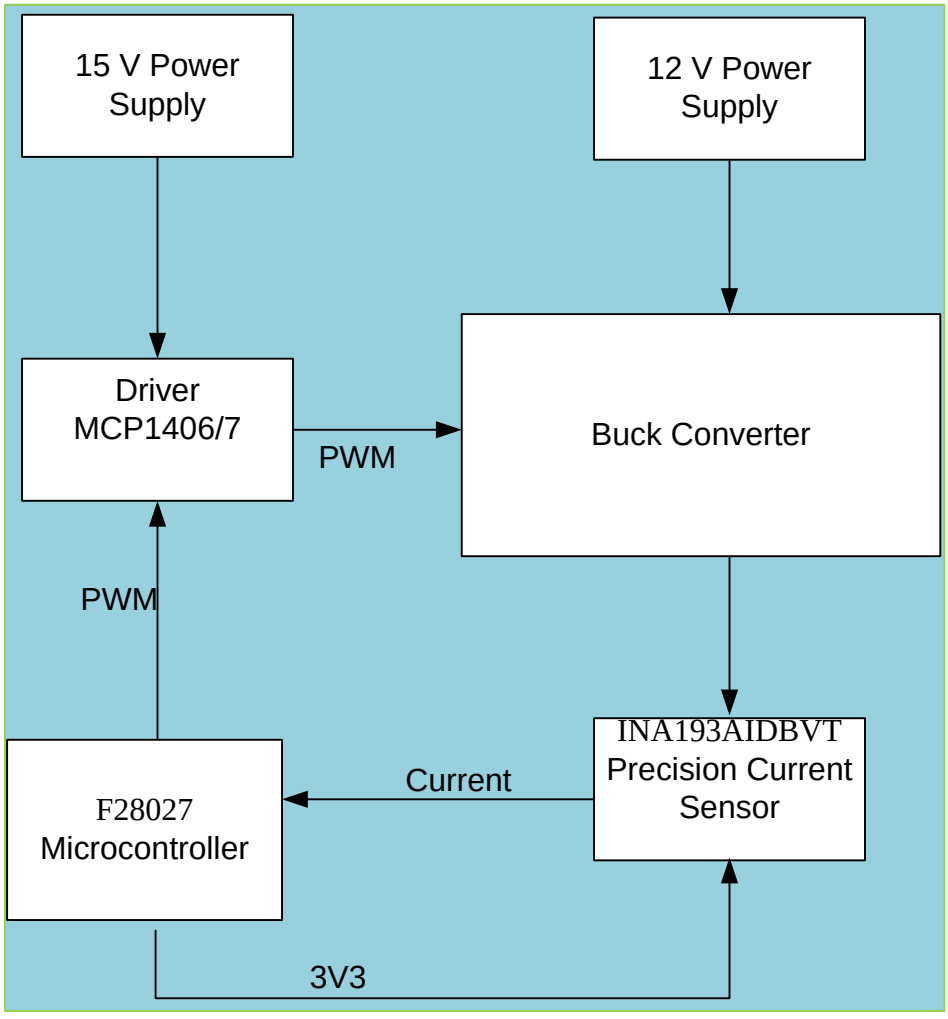

Figure 9: Schematic Diagram of the PCB Board for the Biasing Converter and its Control

3.4.2 Software Implementation of the Biasing Circuit and its Control

The software implementation is performed in C2000™ Piccolo™ LaunchPad™-F28027.This microcontroller is used for ADC conversion of the measured signal, compute the current control and accordingly to trigger the ePWM modules in order to generate PWM signals. The PWM signals from ePWM registers are connected to the MOSFET driver of the buck converter in order to control the switching the gate of the MOSFET switch of the buck converter. The code is developed using C language in *Code Composer Studio v5_4.*

The switching frequency is selected to be 20kHz.Accordingly, the ePWM registers and ADC registers are initialized and configured.

For the software implementation, sequential steps are followed and they are summarized below.

After including the required header files, the prototype statements and global variables are defined. In the main part of the code, all the required handles and system control are initialized. Furthermore, the GPIO pins are enabled and the interrupts are matched to the interrupt service routine (ISR).Subsequently, ADC initialization is followed by the ADC configuration. Then interrupts are enabled and the ADC conversion takes place

The start of conversion is initiated at every zero point. The sampling frequency is the same as the switching frequency. The End of conversion (EOC) triggers the ADC interrupt and the ISR reads and latches the conversion results. The control computations are performed and the output of the controller results are configured to be loaded to the CMPA register to be compared with Time Based Period Register (TBPRD) of the ePWM to obtain the PWM signals to control the switching of the MOSFET.

Internal oscillator is utilized to generate the clock source by setting the PLL and its presale's. CPU clock is set 60MHz.The PWM switching frequency is configured by setting the TBPRD.

CHAPTER 4: Bidirectional DC-DC Converters

4.1.Bidirectional DC-DC Converters

Bidirectional DC-DC converters are key components in interfacing energy sources to the dc-link and power train in traction application. They enable forward and backward flow of power. In the forward power flow mode, power is delivered from the energy source to the motor drive, whilst in the regenerative braking mode, the motor drive acts as a generator, and the inverter acts as a rectifier to charge the energy sources. This concept is vividly summarized in Figure 10.

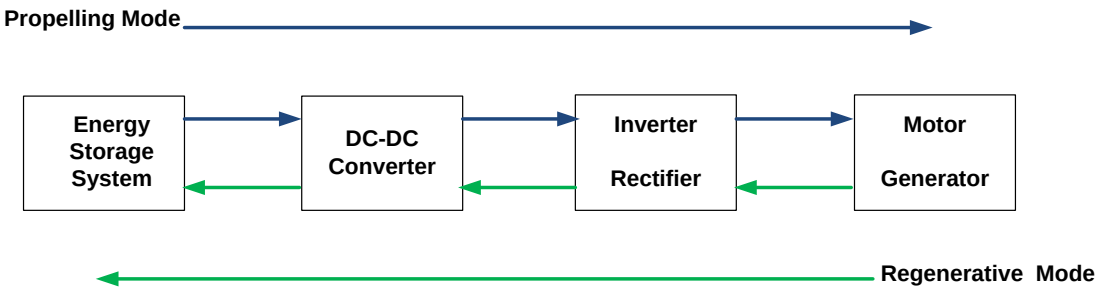

Figure 10: Bidirectional power flow illustration in traction applications

By replacing the diodes in the conventional power converters by MOSFETS and IGBTS, they can be changed into DC-DC converters with bidirectional power flow capability. Bidirectional DC-DC converters in EVs enable the monitoring of power flow in the motoring and regenerative braking modes of operation.

The bidirectional DC-DC converter shown in Figure 11 is a two-quadrant class C DC chopper which enables two way flow of current with positive dc-link voltage. It consists of the energy source, two active switches (IGBTs), power inductor, a dc-link capacitor and a dynamic load to emulate power train of electric vehicles. The energy source could be a battery, supercapacitor, fuel cell, or rectified dc source. The two active switches enable bidirectional power flow and the buck-boost operation. The power inductor has multiple purposes to store energy and deliver energy to the load, and attenuating the current ripples. The main purpose of the dc-link capacitor is to smooth out the dc bus

voltage stability, to prevent ripple currents form propagating to the source and protect power electronic switches [101],[102].

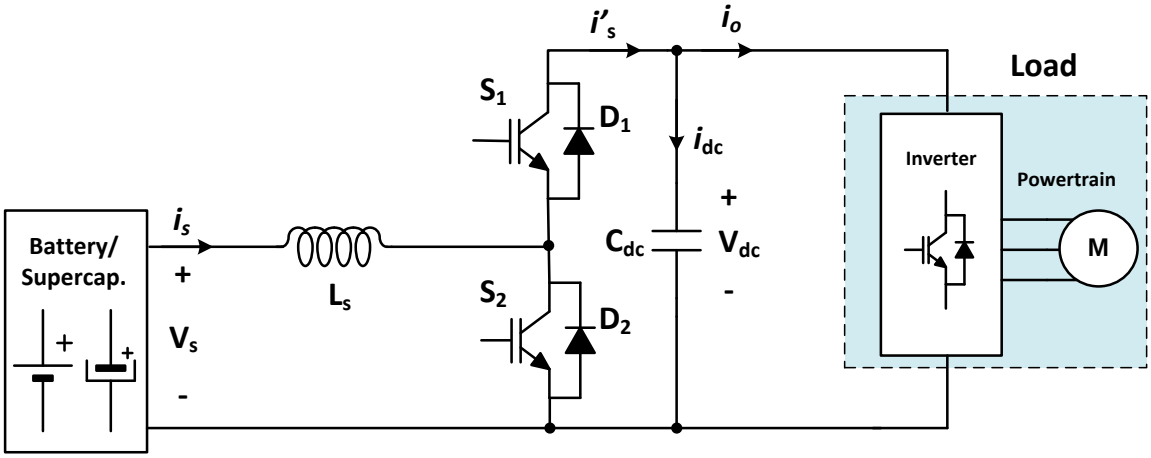

Figure 11: Schematic diagram of bidirectional DC-DC Converter

This topology can be used in boost mode for traction applications during acceleration and hill climbing, and in a buck mode in recharging the battery or supercapacitor in regenerative braking mode [103]. In boost mode, the lower switch and the upper diode are in active state, hence there is power flow from the energy sources to the dc-link and the motor drive. On the other hand, when the upper switch and the lower diode are in active state, power flows in reverse direction that is from the motor to the energy sources that is what we call regenerative braking.

For smooth operation of this topology a robust control strategy is required to monitor the dc-link voltage and to control the to and fro current flow. Both the boost mode and buck mode of operation of the bidirectional converter are summarized graphically in Figure 12 (a) and (b) in respective order. Figure 12 (a) reveals the boost operation mode, IGBT (S2) is on and the inductor charging takes place and the direction of current flow is shown by the blue path. On the other hand, during the discharging phase of the power inductor Diode (D1) is active and the direction of current is shown by the green path. The buck mode of operation is revealed in Figure 12 (b), where the directions of the current paths are changed from the load to the energy sources. When the top switch (S1) is on and the bottom switch (S2) is off current flows from the load to the source through the inductor

as illustrated by the green path. During this time the inductor is charged. When the upper switch (S1) is off, the diode (D2) is on and the energy stored in the inductor is discharged to charge the source and the current flow is shown by the blue path in Figure 12 (b).

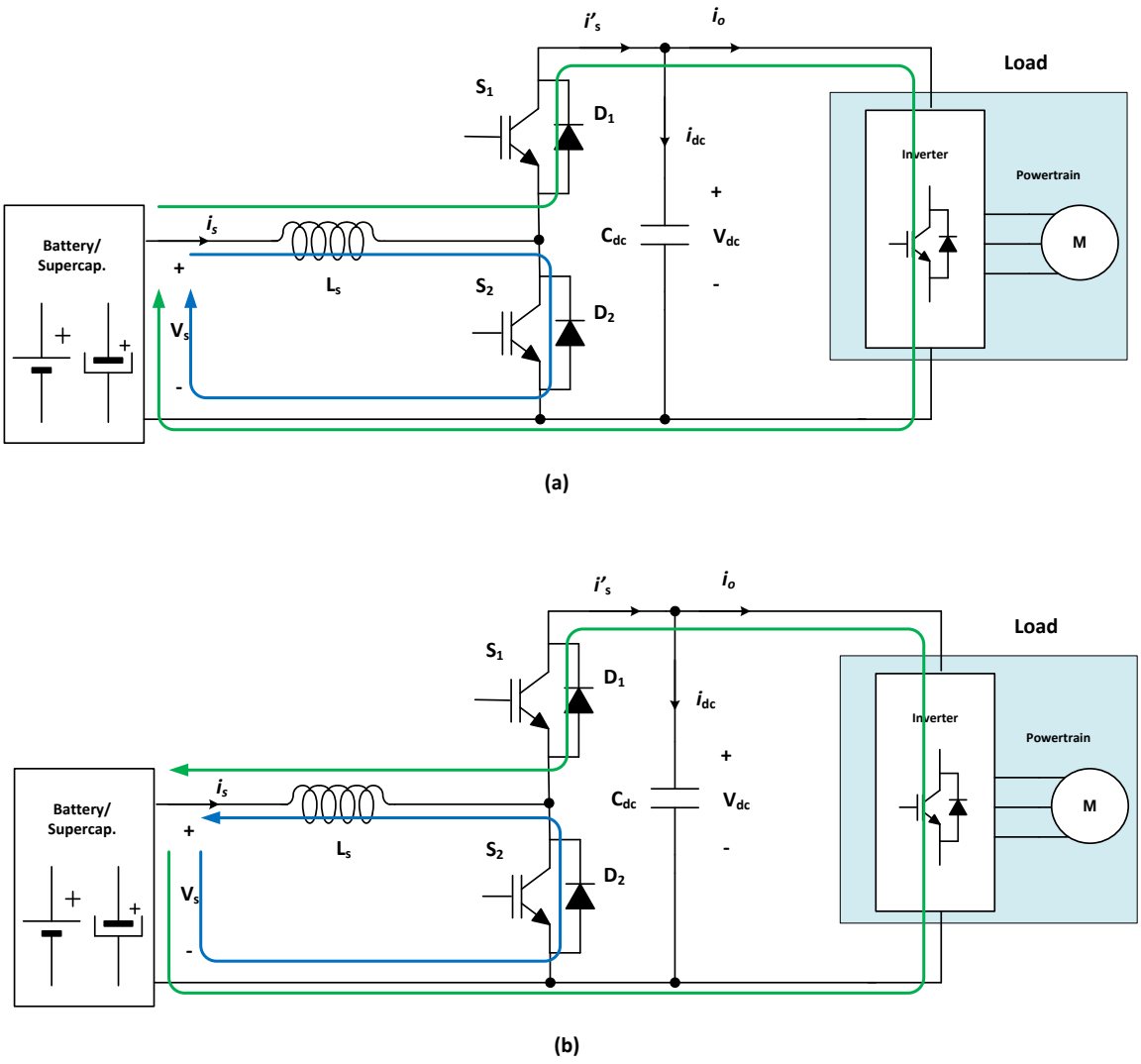

Figure 12: Bidirectional Converter Operating Modes (a) Boost Mode (b) Buck Mode

4.2. Bidirectional DC-DC Converter Parameters and Specifications

From given specifications of a desired application the parameters of bidirectional DC-DC converters can be selected based on the fundamental concepts of design.

In this work, the components are selected based on the components available in the laboratory. The dc link capacitor is chosen based on the ripple voltage of 5% .The

switching frequency is chosen to be 20kHz.The power inductor is a prototype available in the lab, its specifications are determined from experimental observations and measurements. The detailed specifications of the bidirectional DC-DC converter used in this study are provided in Table 3.

Table 3 Specifications and Parameters of the Bidirectional Converter

	Symbol	Value	Unit
Battery Voltage	V_{Bat}	12	V
Dc-link Voltage	V_{dc}	24	V
Inductor Battery Side	L_s	2.148	mH
Dc-link Capacitor	C_{dc}	3.3	mF
PWM switching frequency	F_{sw}	20	kHz

4.3.Average Modeling of Bidirectional DC-DC Converters

For the purpose of this study, battery is considered as a source. As shown in Figure 11, the system consists of an energy source (battery), bidirectional DC-DC converter, the dc-link and an electrical load. All the components and variables are labeled in diagram of Figure 11. The average model can be developed as:

$$L_s \frac{di_s(t)}{dt} = V_s(t) - (1 - d_s(t))V_{dc}(t) \tag{10}$$

$$C_{dc} \frac{dV_{dc}(t)}{dt} = i'_s(t) - i_o(t) \tag{11}$$

Where L_s, i_s, V_s, d_s, V_{dc}, C_{dc}, i'_s and i_o are the buffering inductor, the energy source current, the supply voltage (energy source), the duty cycle, the dc-link voltage, dc-link capacitor, modulated source current and the load current in respective order.

The Laplace transform of the above two equations provides the transfer functions of the plants which we need to control for the proper functioning of the complete system.

$$i_s(s) = \frac{V_{dc}}{sL_s} d_s(s) + \frac{V_s(s) - V_{dc}(s)}{sL_s} \tag{20}$$

$$V_{dc}(s) = \frac{1}{sC_{dc}} i'_s(s) - \frac{1}{sC_{dc}} i_o(s) \tag{21}$$

From the above two equations the state space variables and the control variables are presented in the first terms of the equations and the second terms are disturbances, hence using the concept of feed forward decoupling method, the controllers can be designed and the detailed presentation of controllers design is presented in the following section.

4.4. Controllers Design

The mathematical formulation and average model of the bidirectional converter and the dc-link and load parameters are illustrated in the above section. The design of the controllers for the bidirectional converter and the dc-link are based on the state space representation of the system given in the set of equations (20)-(21). Alike to the biasing converter controller, PI controller is utilized and the controllers gains are calculated analytically from the dynamic model of the system using the same approach used in [98-100].

The first terms in (20) and (21) influence the dynamics of the system and the second terms are disturbances which are not included in this study.

The controllers can be designed based on the set of transfer functions in (24) and (25) which can be obtained from the first terms of the set of equations illustrated above.

There are an outer voltage control loop and inner current control loop. As the current loop is required to have faster response, the bandwidth (ω_{nc}) is selected to be much higher than the bandwidth of the dc-link voltage controller (ω_{nv}).

$$\omega_{nc} = \frac{2 \times \pi \times f_{sw}}{40} \tag{22}$$

$$\omega_{nv} = \frac{2 \times \pi \times f_{sw}}{1600} \tag{23}$$

Considering the first terms of the transfer functions of the bidirectional converter and neglecting the disturbances for the time being, the transfer functions of the bidirectional converter and the dc-link can be expressed as in (24) and (25) in respective order.

$$\frac{i_s(s)}{d_s(s)} = \frac{V_{dc}}{sL_s} \tag{24}$$

$$\frac{V_{dc}(s)}{i'_s(s)} = \frac{1}{sC_{dc}} \tag{25}$$

The above expressions reveal that the dynamics of the converter and the dc-link are mostly influenced by the power inductor and the dc-link capacitor respectively. Since the transfer functions are first order systems. The control strategy can be easily achieved using PI controllers.

The closed loop transfer function of the converter plants and the PI controller plant can be expressed as:

$$\frac{i_s(s)}{i^*_s(s)} = \frac{\frac{Kp^c}{L_s}(s + \frac{Ki^c}{Kp^c})}{s^2 + \frac{Kp^c}{L_s}s + \frac{Ki^c}{L_s}} \tag{26}$$

Where s could be either *Bat* when the battery is considered or *SCs* when a supercapacitor is considered and the superscript *c* is to indicate the gains the PI of the current controller. Comparing expression (14) with the general second order system in (26).The parameters of the PI controllers of the current controller can be calculated by choosing the required natural frequency and damping ratio.

$$K_p{}^c = 2 \times \xi \times \omega_{nc} \times L_s \tag{12}$$

$$K_i^c = L_s \times \omega_{nc}{}^2 \tag{13}$$

Similarly, the dc-link closed loop transfer function can be written as:

$$\frac{V_{dc}(s)}{V^{*}_{dc}(s)} = \frac{\frac{K_p{}^{v}}{C_{dc}}(s + \frac{K_i{}^{v}}{K_p{}^{v}})}{s^2 + \frac{K_p{}^{v}}{C_{dc}}s + \frac{K_i{}^{v}}{C_{dc}}} \tag{14}$$

Using the same approach used for the calculation of the current controllers, the PI gains of the voltage controller are calculated as shown below.

$$K_p{}^{v} = 2 \times \xi \times \omega_{nv} \times C_{dc} \tag{30}$$

$$K_i{}^{v} = C_{dc} \times \omega_{nv}{}^{2} \tag{31}$$

Based on the above modeling procedures, the controllers of the bidirectional converter and the dc-link are designed analytically.

The control structure of the bidirectional converter and the dc-link is depicted in Figure 13. It consists of an inner current loop and outer dc-link voltage loop. The dc-link voltage controller is used to keep the dc-link voltage within the limit so that there is stable voltage to be delivered to the load and prevent current ripple propagation to the source. The reference current for the main winding is obtained from the dc-link controller. The dc-link controller input is the error signal obtained from the desired voltage reference and the actual dc-link voltage. The error signal is processed by the PI controller with gains designed in (30) and (31) to give the reference current required to be delivered to the load.

The current controller processes error signal obtained from the difference of the reference current and the actual measured current and accordingly provides control signals. The output of the current controller is limited through saturation blocks in order not to exceed the rating of devices and the output is used as a reference signal to generate the PWM signals for controlling the power electronic switches of the bidirectional converter.

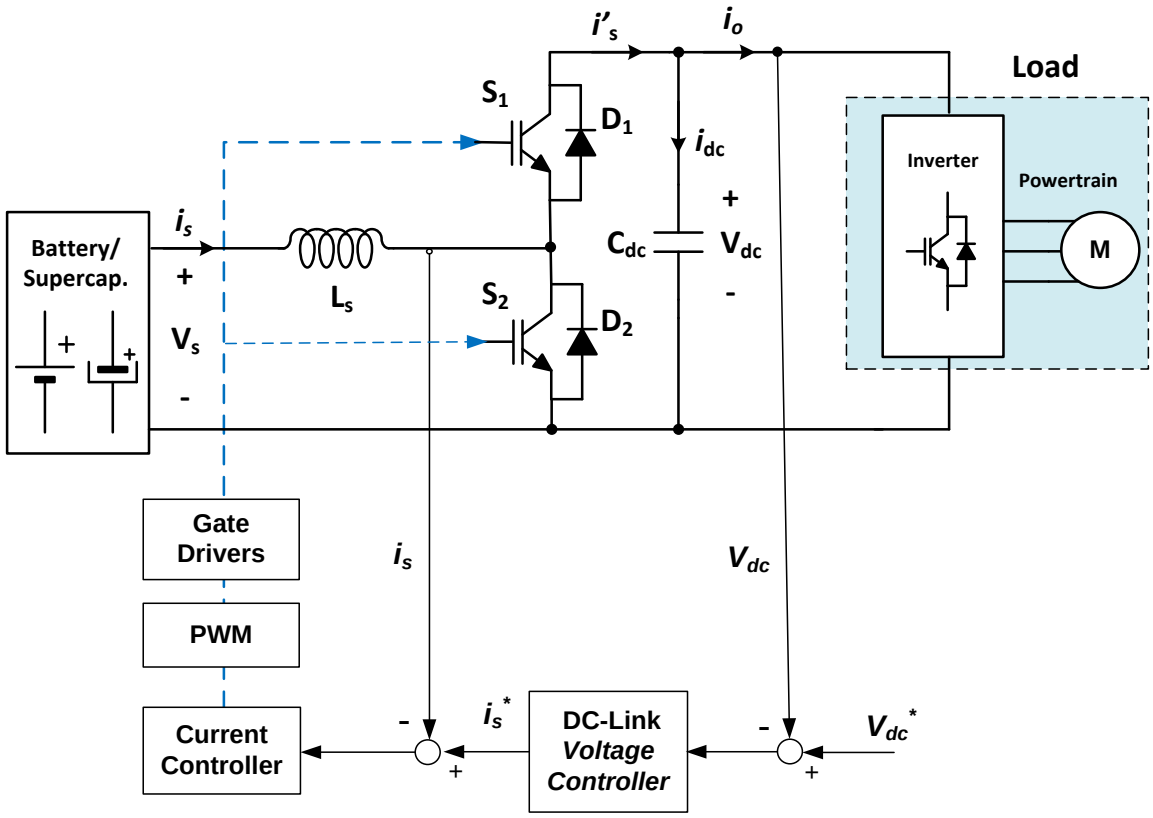

Figure 13: Bidirectional Converter and its Control Structure

4.5. Bidirectional DC-DC Converter Simulation Results

In order to understand the operation of the bidirectional converter and to validate the designed controllers extensive simulation studies are carried out in *MATLAB/Simulink*. The performance of the dc -link control and the current controller of the bidirectional converter under investigation are evaluated with simulation prior to the hardware implementation.

To emulate different driving cycles in EVs, a variable load with a characteristic curve shown in Figure 14 is connected at the output of the bidirectional converter. The characteristic curve is used to simulate different driving cycles in the propelling mode and regenerative modes of operation. At the onset of the simulation period the EV is assumed to be at rest for the first second. Then the load is increased in steps of 1kW for the next two steps and further increased to 4kW. With the variations of the load, the dc-link controller acts in order to enable the measured voltage to track its reference value

and maintain the dc-link voltage with in safe operation limits. At t=3 seconds a considerable voltage undershoot is noticed in the dc-link, due to hard acceleration, which mandates the dc-link to provide more current, hence the voltage falls to counteract this variations. Nevertheless, the observed undershoot is no more than 10%.Therefore the dc-link controller performance is quite successful. On the other hand, at t=4 seconds, the dc-link voltage is increased and an overshoot in the dc-link voltage is noticed. Basically, this is due to the sudden fall in the load requirement, the current from the source is leading to the dc-link voltage build up. But in all the cases the increase and decrease of the dc- link voltage are within the safe limit, which validates the proper functionality of the dc-link voltage controller.

Similarly, the reference current and the actual current form the battery are shown in Figure 15 (b) and it is not easy to identity each of them, which validates the successful performance of the current controller. In the first three seconds, the currents follow the pattern of the load change and both currents align perfectly. Similar to the transient effect in the dc-link controller.

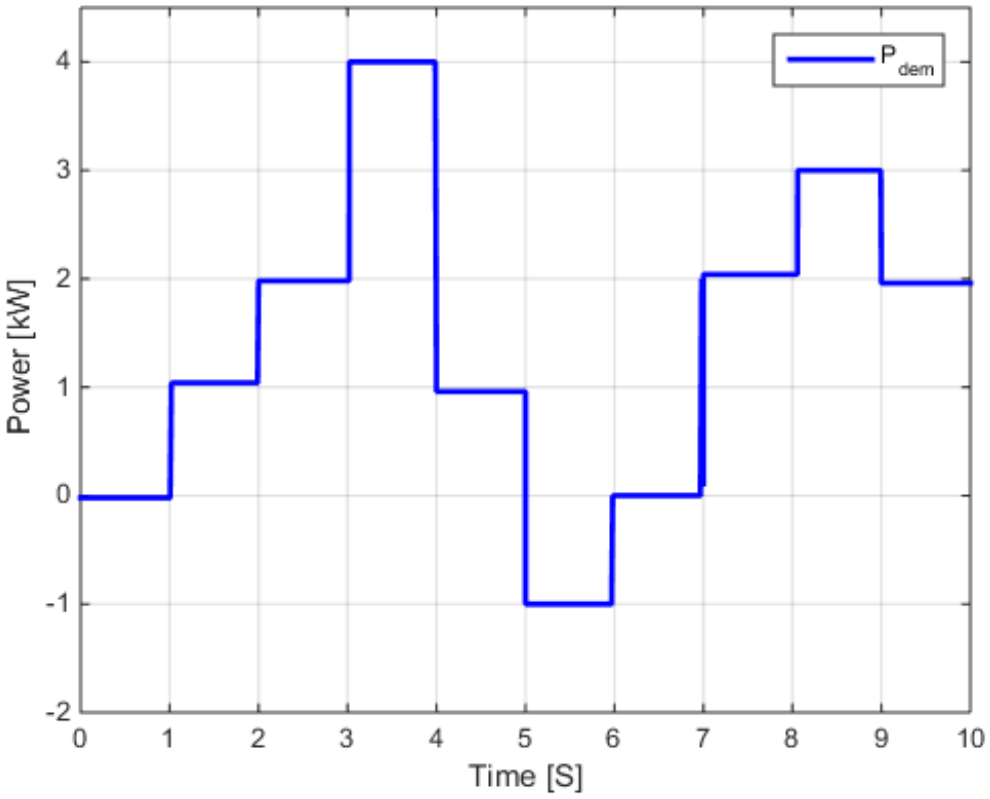

Figure 14: Load Power Characteristics Curve

At the end of the fourth second, the load power starts to fall to 1kW and then further reduced to -1kW in the fifth second. This is to show that the car is ascending from a hill, in this situation the wheels of the car rotate the motor and the motor acts as a generator. The energy regenerated from the load is delivered to the energy source, hence the direction of the current flow is negative as clearly shown in Figure 15 (b) in the interval [5 -6] seconds.

In the interval [6-7] seconds there is no power requirement of the load hence there is no current delivered from either side. Again the power demand of the load is increased from zero to 3kW in the next two cycles and finally dropped to 2kW to simulate different driving cycles in real applications.

It has to be noted that, the current controller is designed to have faster transient performance than the dc-link controller. This is validated from the zoomed pictures of the

waveforms. In the voltage wave forms, the measured signal takes little time to track its reference but the current signal tracks its reference immediately.

Finally, several steps are simulated in order to test the robustness of the designed controllers. Accordingly, it can be deduced that the designed controllers demonstrate successful performance within the design specifications.

.

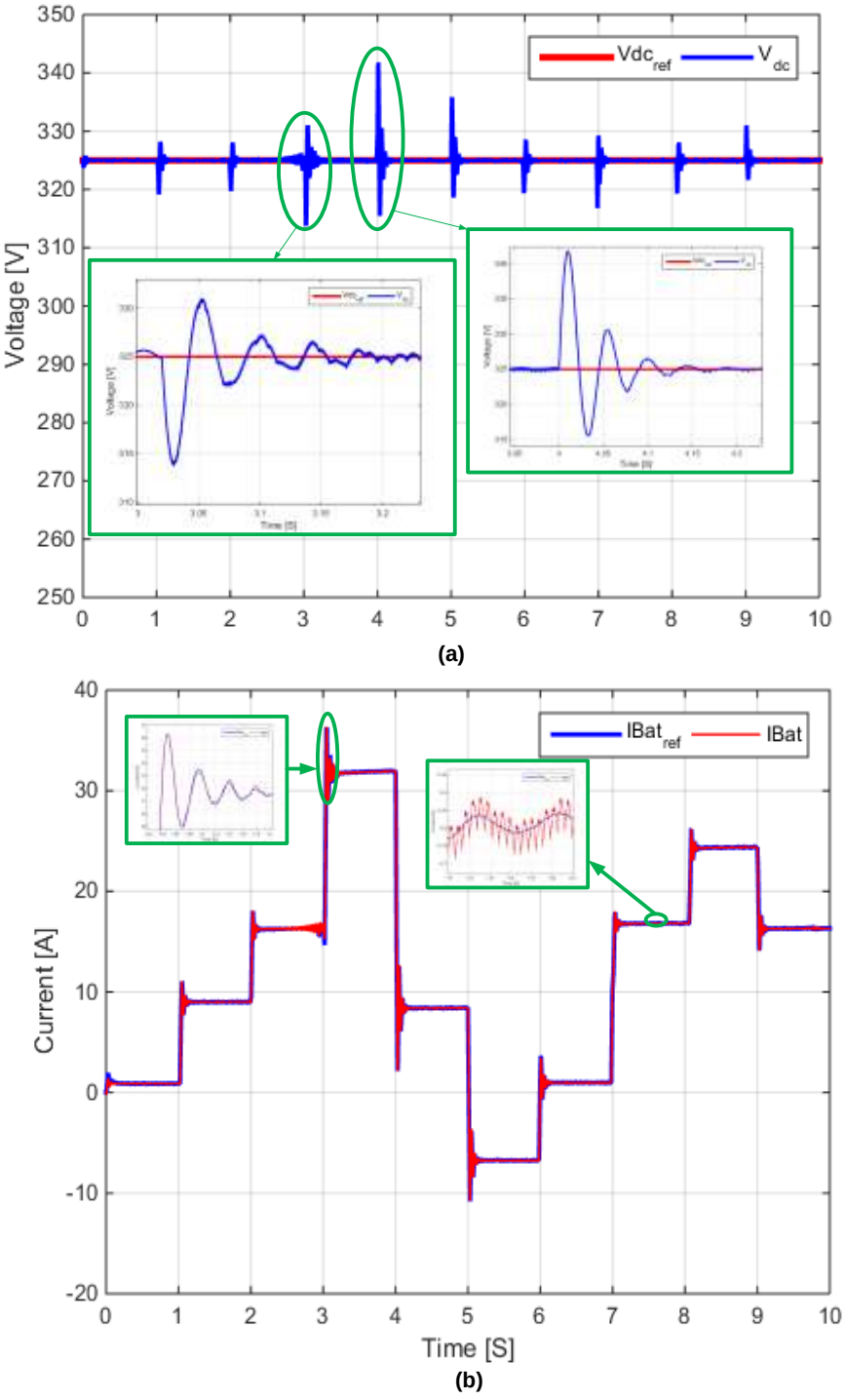

Figure 15: Simulation Results of Bidirectional Converter (a) dc-link voltage (b) Battery Currents

CHAPTER 5: Study System Summary and Results

5.1. Global System Description

The diagram in Figure 16 reveals the detailed overview of the overall system considered in this study. It consists of the bidirectional DC-DC converter where the conventional power inductor is replaced by the VI, the dc-link capacitor, the load, the biasing converter and the power control layer. Each part is illustrated in different parts of this work. It is included here so as to give a tacit summary of the overall study system used in simulations and experiments.

The power control layer is composed of a cascaded voltage and current controller for the bidirectional converter and current controller for the biasing converter. The dc-link voltage controller maintains the dc-link voltage within the limits and provides the reference current and the main current controller regulates the actual current in the main winding.

The reference current for the current controlled buck converter is obtained from the control current estimator block. The current estimator block determines the reference control current based on the levels of current in the main winding. The relationship between the main winding current and the control winding current is based on a lookup table obtained using curve fitting toolbox in *MATLAB* from a series of tests. The current controller of the biasing winding, senses the levels of the main winding current and acts accordingly in order to control the saturation level of the main winding or the current ripple. The complete control system is implemented in C2000™ Piccolo™ LaunchPad™-F28027 Microcontroller. For the biasing converter the closed loop is implemented and its functionality is validated. For the bidirectional converter, an open loop control is used to analyze and characterize the operation of the system with VI. Then from a series of tests in open loop the relationship between the control winding current and main winding current is obtained using curve fitting toolbox in *MATLAB.* After analyzing the system and obtaining the relationship between the two currents, the closed loop control is implemented and tested.

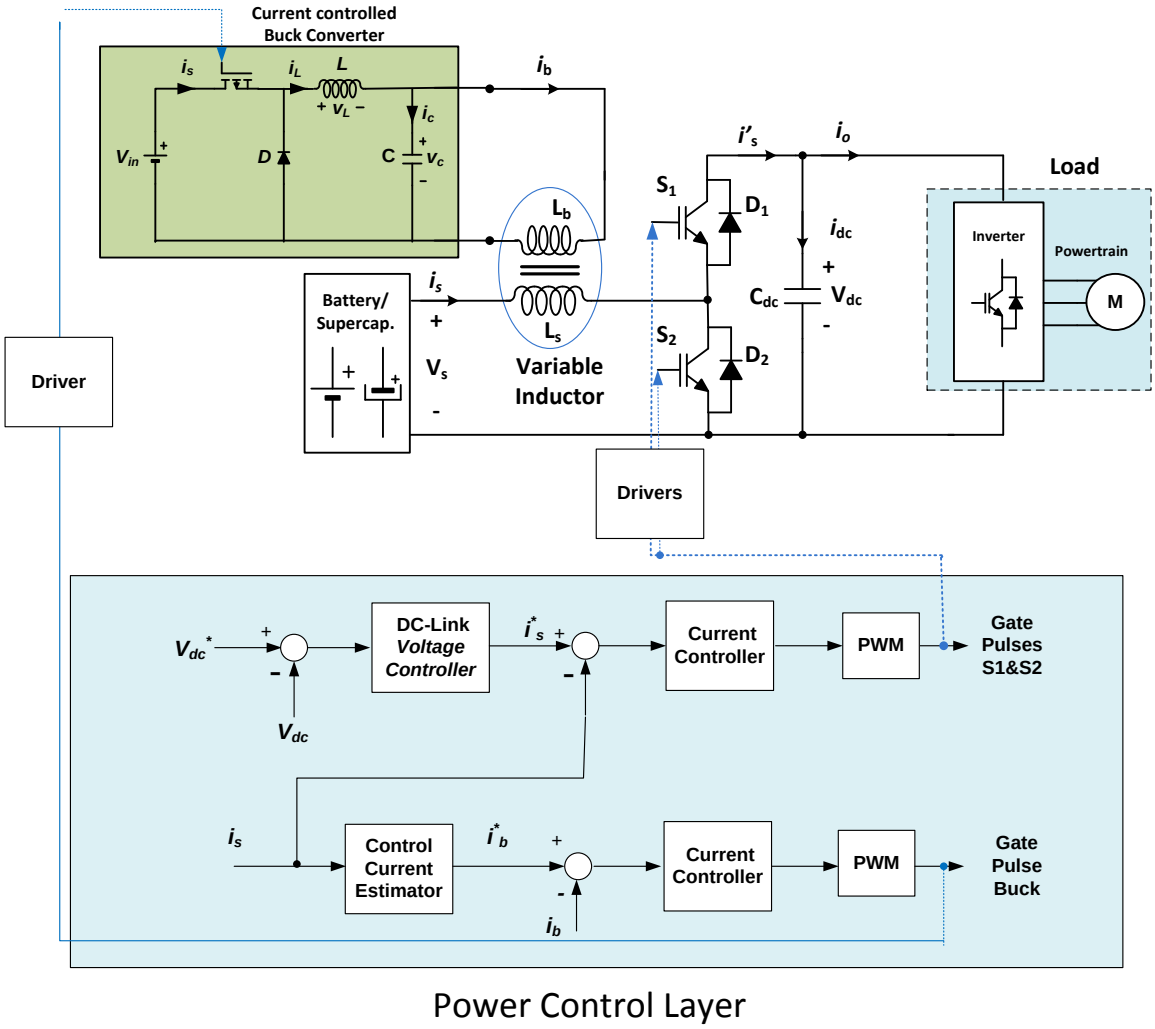

Figure 16: Global Study System

5.2.Experimental Demonstration

This section provides the experimental results of the improved bidirectional converter realized with VI. Replacing the saturating power inductor by the proposed VI improves the performance of the converter, controls the amount of ripple current and enhances the saturation level of the magnetic core. Therefore, this section provides the small signal characterization of the VI and illustrates the improvements obtained with the introduction of VI in bidirectional converter.

5.3. Description of Experimental Setup

The experimental set up consists of a bidirectional DC-DC converter, a current controlled buck converter, a dc-link capacitor, power supplies, RLC meter and C2000 launch pad TMS320280273 Piccolo platform.

The bidirectional DC-DC converter used is a half-bridge IGBT topology operating in continuous conduction mode powered by battery pack. The double arm half-bridge IGBT set is from Semikron (SKM 100GB063D, 1200V, 100A) and the driver is from the same manufacturer (SKYPER 32 PRO R). The driver has several functions such as driving, potential separation, protection and interfacing between the IGBT and controller. A C-snubber is used to suppress overvoltage in the terminal of the power module. For interfacing the measurement signals to the microcontroller and the control signals to the IGBTs of the half-bridge bidirectional converter an interface PCB is manufactured.

In the implementation of the bidirectional converter, the conventional power inductor is replaced with the VI prototype realized with two windings available in the lab. The principle of operation of VI is illustrated in the previous chapters. The control winding of the VI is powered by a small and low-power buck converter. The buck converter is realized in PCB and its controller is implemented in the Microcontroller.

The dc-link capacitor is from KEMET with 3.3mF, 400V (KEMET ALS31A332NF400). To emulate the dynamic behavior of the load in EV, two batteries connected in series are used as a load.

The control and automation of the system is performed in a C2000 launch pad TMS320280273 Piccolo platform. In order to interface the actual signals two current sensors and one voltage sensor are utilized. The current sensor for the biasing converter is an INA193AIDBVT precision current sensor and the main inductor current sensor is an ACS758LCB-050B-PFF-T from Allegro™, this current sensor is very noisy and it creates a lot of problems in testing of the closed control of the overall system. To reduce the noise level, a 470nF filter capacitor is used. This filter reduced the noise level, but it cannot eliminate it hence introduced instability in the current controller.

An LV 25- voltage sensor from LEM is used to measure the dc-link voltage. Accordingly, these signals are processed in order to obtain the control signals for the switches of the converters under study.

The biasing converter, power and control interfaces are implemented in printed circuit board (PCB). With the utilization of separate ground planes connected at a point, the noise and capacitance effects are minimized in the PCB. And a separate PCB is used for interfacing the signals and control of the bidirectional converter. This PCB consists of the voltage sensor for the dc-link voltage and two gate drivers and optocouplers.

The complete set up of the experimental system is depicted in Figure 17.

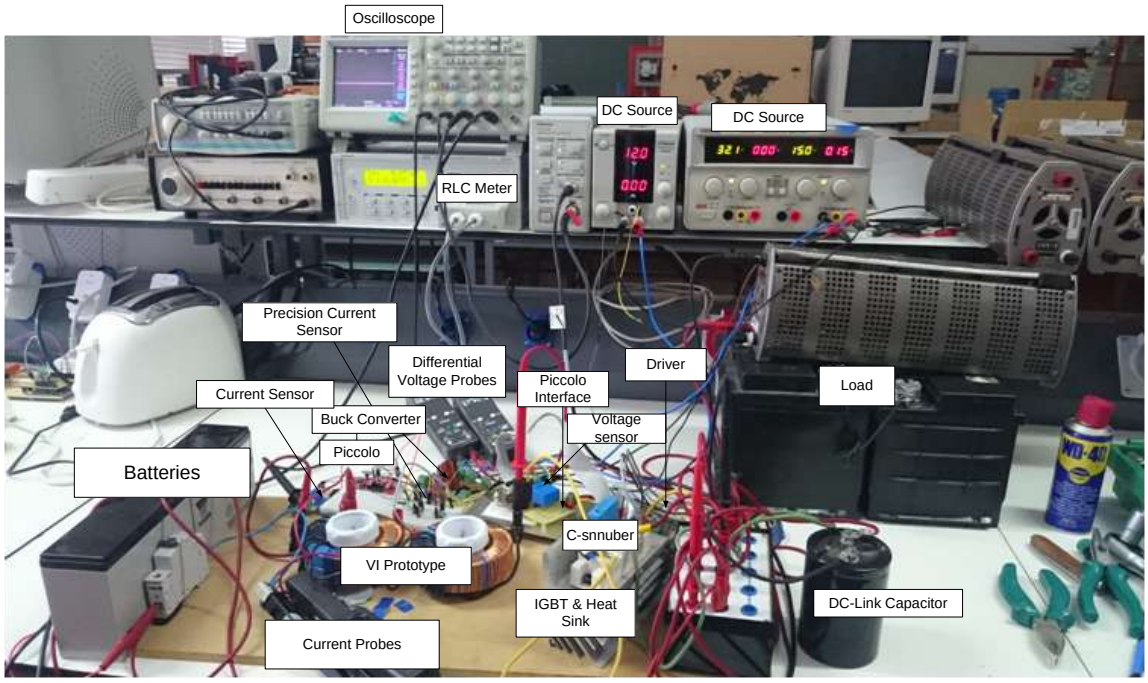

Figure 17: Experimental Setup

5.4.Experimental Results

To verify the validity of the proposed concept of VI in traction applications a number of tests are performed. The tests are focused on the investigation of the VI characterization, functionality of the biasing converter and its control, and the improvements obtained due to the introduction of the VI in bidirectional converter.

5.4.1 Small Signal Characterization of Variable Inductor

Small signal characterization refers to the variation of the inductance of the power inductor due the change of small dc biasing current applied to the control winding. Magnetizing a power inductor with dc current leads to the saturation of the magnetic core. The saturation of the magnetic core in turn results in the reduction of the inductance of the power inductor.

The small signal (dc bias) characteristics of the power inductor is performed by applying a small dc bias current to the control winding of the VI and connecting the main winding to an RLC meter. The biasing current is made to vary by the duty cycle of the current controlled buck converter and the main winding inductance is measured for each value of current. Accordingly the results are recorded and the small signal characteristic curve of the power inductor is obtained by plotting inductance vs biasing current in *MATLAB*. The schematic of the experimental set up for small signal characterization is depicted in Figure 18. It is composed of the current controlled buck converter, the biasing winding, the main winding and an RLC meter.

The experimental results and small signal characterization curve of the VI are shown in Table 4 and Figure 19 in respective order. Both open loop and closed loop current variations are considered and closed loop provides more precise results as it enables commanding of the desired current with a reasonable precision. Therefore, the closed loop results are utilized to get the small signal characterization of VI.

From the small signal characterization curve and Table 4, it can be observed, small dc current in the control winding can lead to saturation of the power inductor hence, its inductance is falling drastically. With a controlled current of 50mA, the inductance rolls to about 74% of its initial value and with about 150mA, the inductance value is reduced to 26% of its initial value. With higher dc bias currents the inductance rolls down very fast which validates the dc bias characteristic of power inductors reveals the rolling down effect of the inductance of power inductor with the dc bias current.

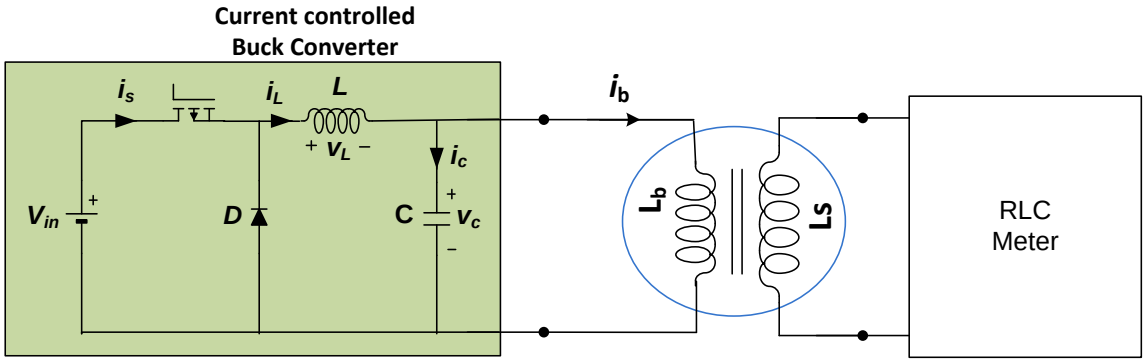

Figure 18: Schematic Diagram for Small Signal Characterization of the Power Inductor

It should be noted that with no current in the main winding, the inductance value of the main winding is observed to fall with the increase of control current due to the reduction of permeability of the magnetic material. If the VI is placed in the bi-directional converter for typical operation, the inductor will respond according to the combination of both currents (control and main current).

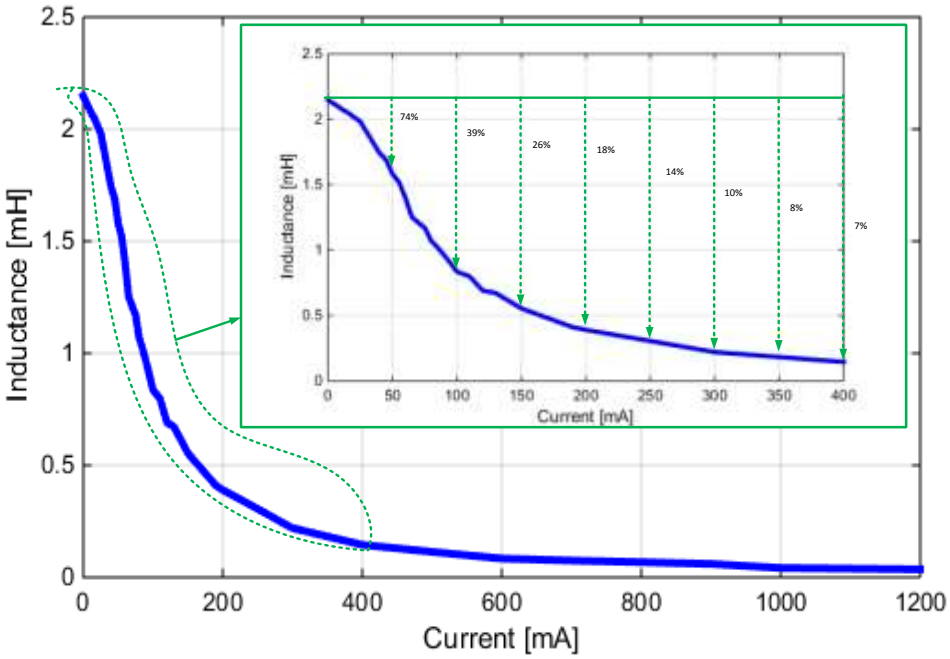

Figure 19: Small Signal Characterization of Variable Inductor

Table 4 Small Signal Characterization Experimental Results

Open loop Results		Closed Loop Results	
Io (mA)	Lo (mH)	Ic (mA)	Lc (mH)
0	2.14	0	2.148
13.58	2.059	13	2.062
14.98	1.757	14	2.06
23.98	1.6748	25	1.982
42.98	1.51	40	1.74
73.98	1.133	45	1.69
105.18	0.5501	50	1.58
186.18	0.4	55	1.52
228.18	0.3041	60	1.4
271.18	0.2408	65	1.253
282.18	0.2252	70	1.21
313.18	0.19808	75	1.17
356.18	0.16732	80	1.07
397.18	0.14512	85	1.02
440.18	0.12803	90	0.962
483.18	0.11516	95	0.9
526.18	0.10454	100	0.835
568.18	0.09521	110	0.798
611.18	0.08825	120	0.69
675.18	0.08154	130	0.672
720.18	0.07553	150	0.554
767.18	0.07005	190	0.41
815.18	0.06835	200	0.39
862.18	0.06297	300	0.22
905.18	0.06043	400	0.145
950.18	0.05707	500	0.114
1000.18	0.05452	600	0.084
1040.18	0.05222	700	0.075
1090.18	0.05019	800	0.068
1130.18	0.04842	900	0.06
1180.18	0.04669	1000	0.042
1270.18	0.04391	1200	0.036

5.4.2 Overall System Experimental Results

The experiments in this section are focused on the global system in order to clearly understand the effects and improvements due to the introduction of the VI concept.

To quantify the improvements, it is very critical to study the system characteristic without the utilization of the VI. In order to do so, the main winding current is varied until the saturation current is reached and beyond to quantify and describe the effects of saturation. Accordingly, it is found that operating the power inductor above the saturation limit leads to more loses and increases the current ripple. This was manifested with the heating

of the switching device, an audible noise in the power inductor and changing the shapes of the current waveforms.

The experimental results are summarized in Table 5. It can be clearly shown that the increase of current in the main winding results in more ripple. Increasing the duty cycle from 0.5 to 0.65 increases the peak-to-peak ripple significantly, the ratio of the current ripple reaches about 90.16% at D=65%. Such a high ripple results in more losses hence affects the efficiency and performance of power converters. This describes the typical behavior of such converters for traction applications if the power inductor in the converter is pushed to its limits.

Table 5 Effect of Increasing the Main Current on Current Ripple

Duty Cycle	$I_{L(rms)}$	$I_{L(av)}$	Peak to Peak Ripple	Ripple (%)
0.50	3.94	3.77	1.6	42.44
0.52	3.96	3.94	1.76	44.67
0.58	6.3	6.24	3.6	57.69
0.62	8.81	8.25	6.8	82.42
0.63	9.39	9.22	8	86.77
0.64	11.5	11.3	9.8	86.73
0.65	12.8	12.2	11	90.16
0.70	16.2	15.8	13.8	87.34

The inductor starts to saturate when the root mean square (rms) current across the inductor is 6.3A at D=0.58, in this situation the current ripple is about 57.69%. Further increasing the main winding current to higher values, the amount of ripple current is observed to increase up to 90% at D=0.65 with a noticeable noise in the power inductor and heating of the IGBT.

The waveforms obtained from the a series tests to characterize the amount of current ripple with the increase of current are presented in Figure 21, for small currents in case of (a)-(c), the inductor is operating under normal condition, hence the ripple current is within the limit. However, for currents above the saturation current the current ripple is higher and reaches to about 90% in (e)-(f).

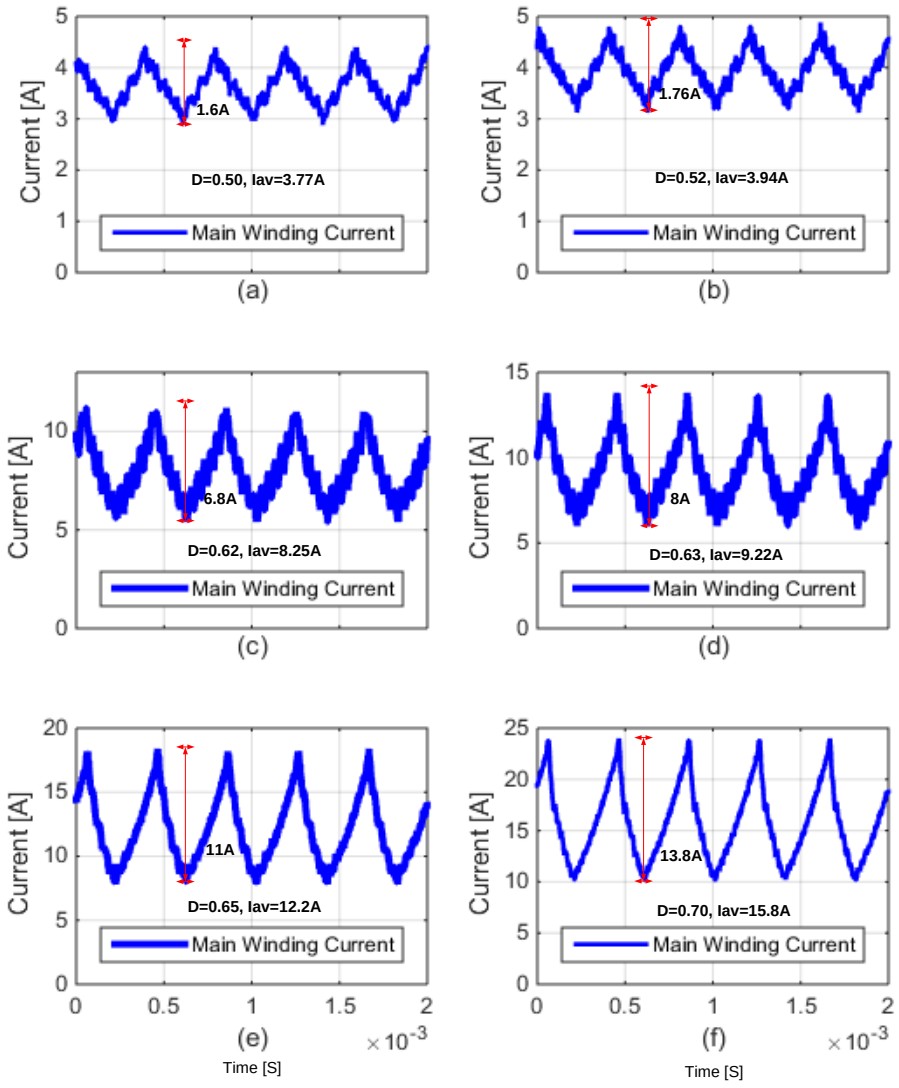

Figure 20: Current ripple variations in power inductor due to the increase of current in the main winding

The percentage of ripple variation with different values of duty cycle and the main winding currents variation is depicted in Figure 21 (a) and Figure 21 (b) respectively. Figure 21 (b) shows the average current, rms current and the peak to peak ripple variation of the main winding current. As it can be clearly shown the magnitude of the ripple percentage is lower for smaller currents and higher for larger currents. The gap between the average current, the peak to peak ripple shows this variations vividly.

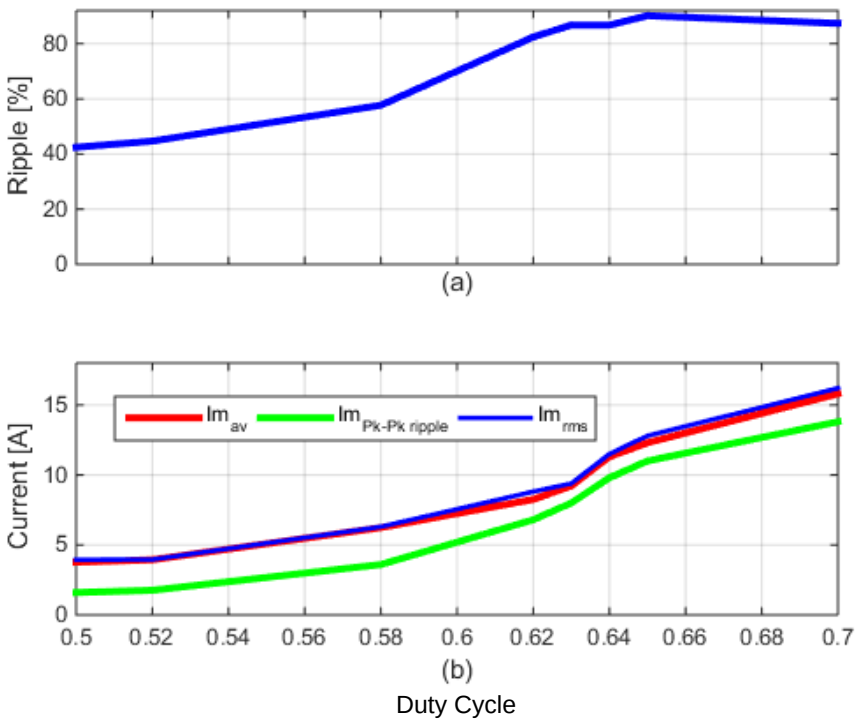

Figure 21: Ripple Current Variation and main winding currents with the increase of Duty Cycle

After carefully analyzing the characteristics of the power inductor with the increase of current in the main winding, the control winding is activated and made to deliver controlled current to the bias winding in order to control the inductance of the main winding, hence to control the amount of current ripple. As clearly shown in Figure 20 (e) and (f), the percentage of ripple currents are 90% and 87.34% respectively. For these two cases, correction actions are taken by applying controlled bias current to the biasing winding.

The biasing winding is configured in such a way that to cancel out the main flux. The interaction of the main winding flux and the bias winding flux influences the permeability of the material hence the inductance of the inductor. Canceling part of the main flux enhances the saturation level of power inductor and reduces the amount of current ripple.

For D=65%, the ripple current is 90% when no control current is applied to the biasing winding. However, if a control current is applied, a remarkable reduction of current ripple is observed. The control current is varied from 0-1A and the changes in the amount of current ripple are shown in Table 6 and Figure 22.

With the increase of the control current, there is a considerable current ripple reduction, due to the cancelation of the main winding flux by the control winding flux, which in fact enhances the saturation level of the magnetic core. For instance for the control current of 0.85A, a considerable current ripple improvement of 40% is achieved as shown in Table 6 and Figure 22 (c). Besides it can be observed that by utilizing the control winding, the saturation level of power inductor can be enhanced and the power inductor is safely operating for a current double of its saturation current limit.

The VI is again tested with larger currents and the inductance is varied with the controlled current, certainly a remarkable current ripple reduction is observed but the biasing winding flux is not enough to overcome the saturation effect. Distortion in the current waveform, noise and heating of the IGBT is observed for this larger current. Though the device is operating in saturation mode, the ripple current is improved by 47% and the average current is increased.

Therefore this test results reveal the promising suitability of VI for current ripple reduction for currents above the saturation level.

The results are summarized in second part of Table 6 and Figure 23.The applied bias current is indicated in the left side and the corresponding main winding current in the right side. For a control current of 0.45A, the amount of peak to peak current is reduced from 13.8A to 12.4A .Similarly, with a control current of 0.85A, the peak to peak ripple current is reduced to 10A and the average current is increased to 17.4A from 15.8A.

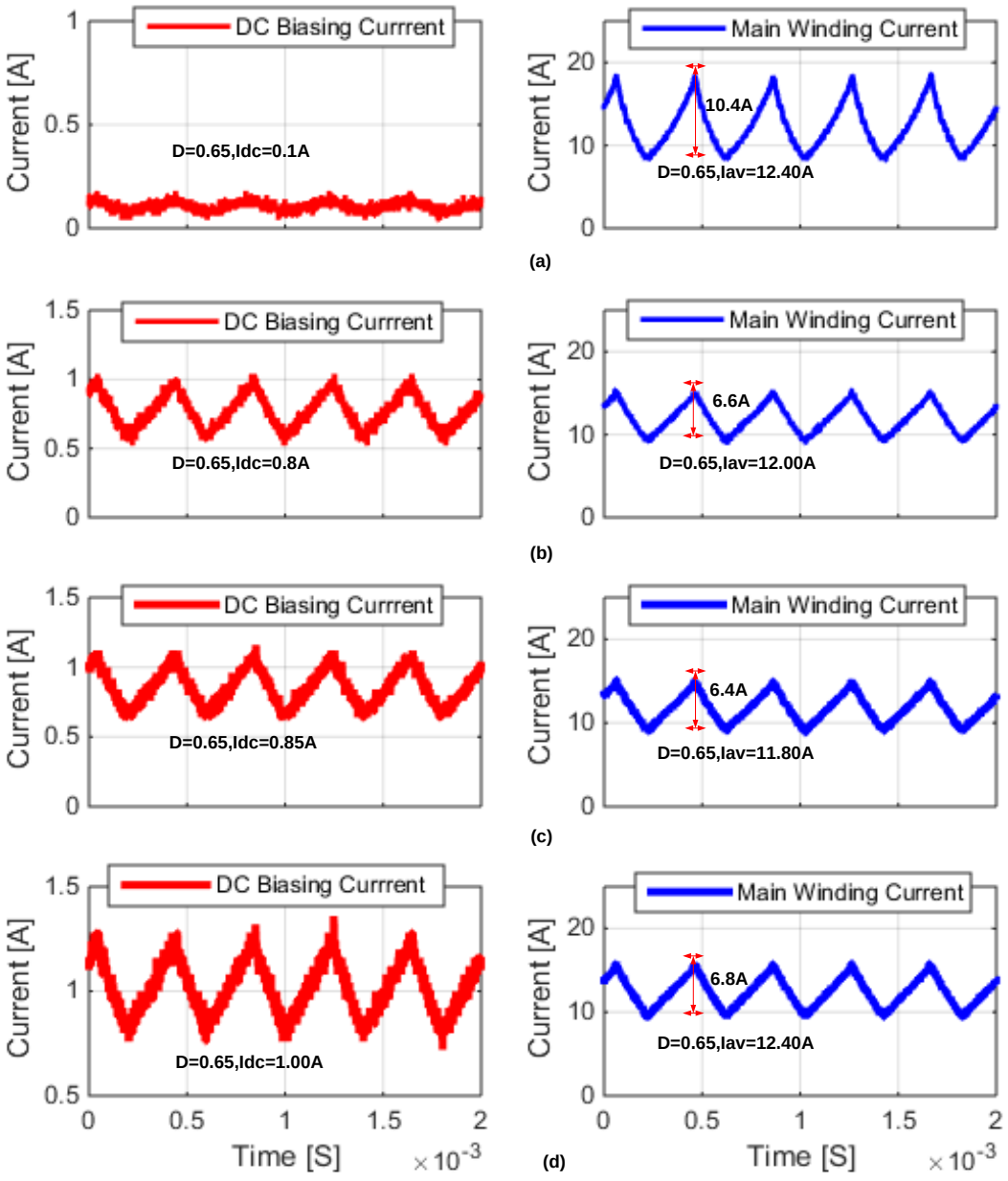

Figure 22: Experimental results for Duty Cycle (D) =0.65 and different control currents in the biasing winding

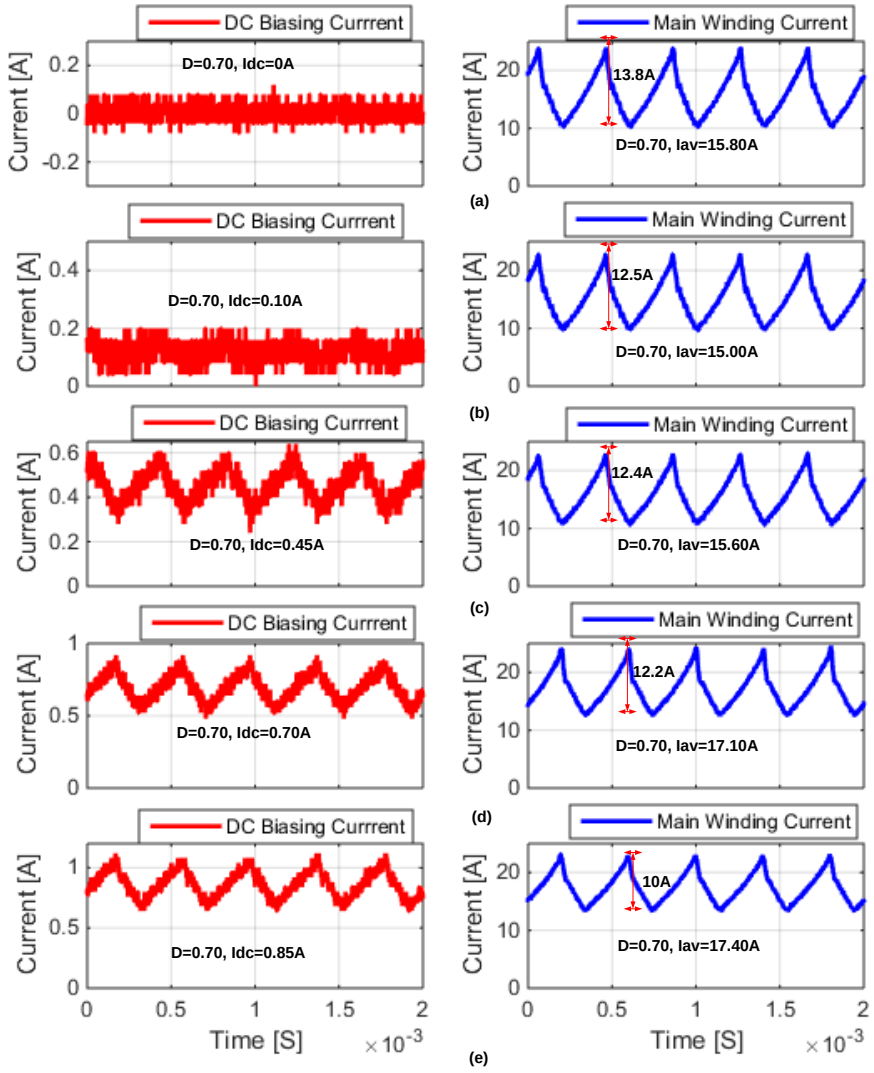

Figure 23: Experimental results for D=70% and different control currents in the biasing winding.

Table 6 Effect of the Biasing Current on Current Ripple Improvement

Idc (A)	$I_{L(rms)}$(A)	$I_{L(av)}$(A)	Peak to Peak Ripple (A)	Ripple (%)	Ripple Improvement
D=0.65, Average Inductor Current=12.2A, Peak to Peak Ripple=11A, Ripple (%)=90.16					
0.1	12.67	12.4	10.4	83.87	7%
0.45	12.3	12.1	8.4	69.42	23%
0.7	12.5	12.4	7	56.45	37%
0.8	12.1	12	6.6	55.00	39%
0.85	11.9	11.8	6.4	54.24	40%
1	12.5	12.4	6.8	54.84	39%
D=0.70, Average Inductor Current=15.8A, Peak to Peak Ripple=13.8A, Ripple (%)=87.34					
0.1	15.4	15	12.5	83.33	5%
0.7	17.4	17.1	12.2	71.35	18%
0.85	17.6	17.4	10	57.47	34%
1	17.1	17	7.8	45.88	47%

With the proposed VI, a very considerable ripple current reduction improvements are obtained. These are summarized in Figure 24. It is shown that applying controlled current of 0.85A to the control winding about 40% current ripple reduction is obtained for D=0.65 and similarly by using 1A controlled current, the ripple current is reduced to 45.88% which indicates 47% reduction when compared with the situation where there is no control current.

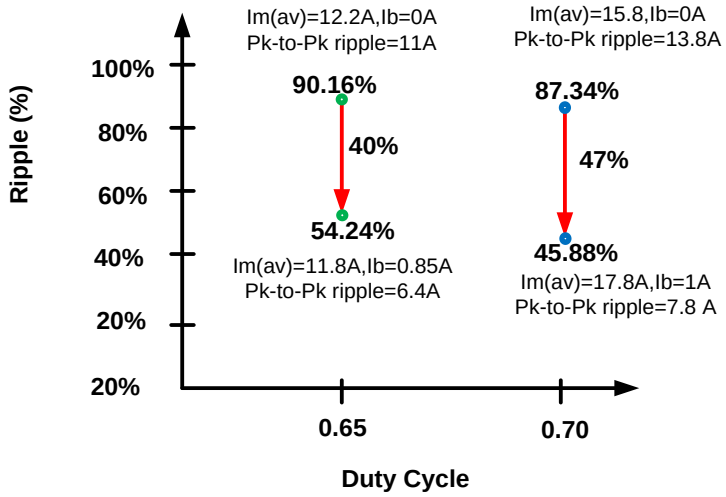

Figure 24: Graphical representation of ripple current improvements.

the above results are obtained from open loop operation of the bidirectional converter and closed loop operation of the buck converter. In practical applications, the overall system should operate in closed loop and the current estimator of the buck converter should be linked to the main winding current in order to regulate the inductance of the main winding in accordance to the levels of main winding current.

In fact, the relationship between the control winding and the main winding is obtained from a series of tests. The current levels which are optimal for each level of current are obtained from a series of tests accordingly the results are processed in *Curve Fitting Toolbox in MATLAB*, accordingly this is programmed in the microcontroller. When the reference current is changed the reference current of the biasing winding changes according to the level of current in the main winding. The current control current estimator block senses the main winding current and according to the relation obtained in the from the Curve Fitting Tool, provides control current reference to the control buck converter in order to reduce current ripple and enhance the saturation level. If the saturation level is not enhanced, it enables controlling the levels of current ripple in the main winding.

Some of the experimental results of the closed loop operation of the system are revealed in Figure 25. In each Figure, the control winding current is revealed in the left side and its corresponding reference and actual currents are shown in the right side. As it can be clearly shown in Figure 25 , the closed loop control and the control strategy to relate the two currents provides superior performance compared to the open loop. With the closed loop the ripple percentages for different currents are less compared to their open loop counterparts.

Figure 25 (a) and (b) shows the controlled current reduces the ripple level and the saturation level is enhanced. This situation is revealed in the waveforms. However, in the last two pictures, a remarkably significant ripple current reduction is observed but still the power inductor is operating in the saturation region of the B-H curve, the main current waveforms reveal this situation clearly.

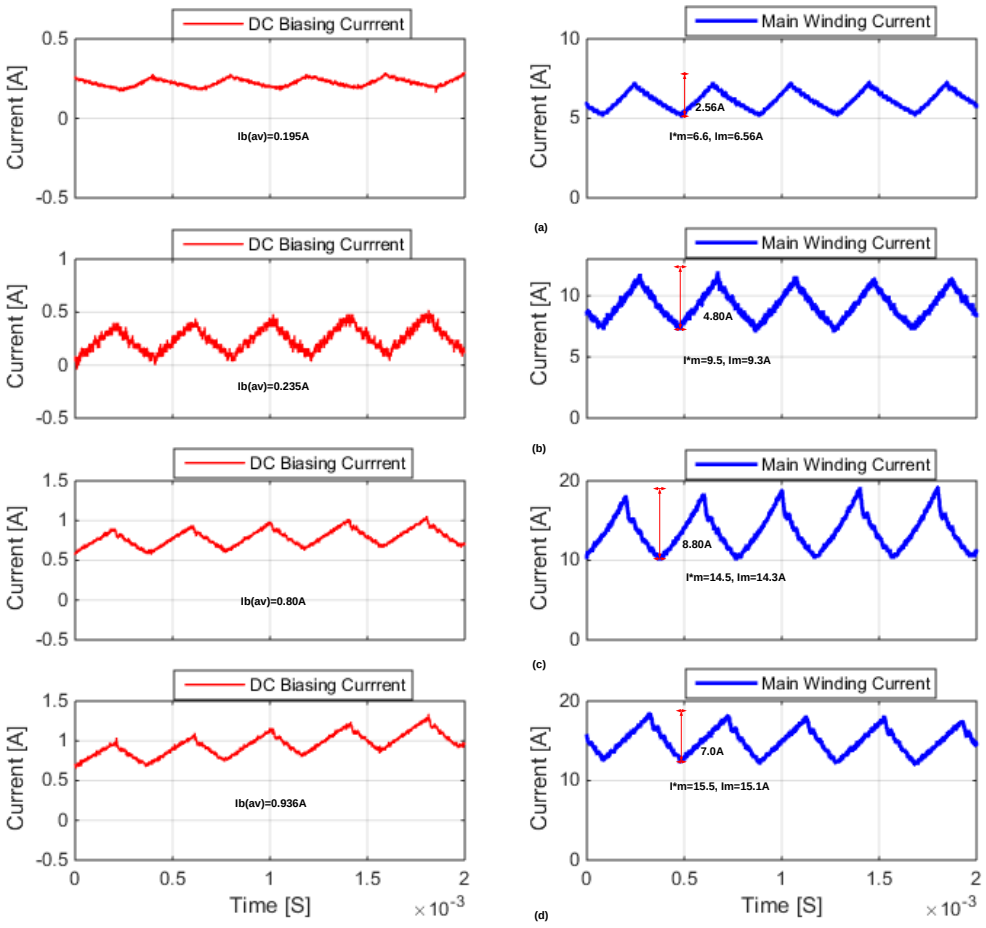

Figure 25 Closed Loop Results

5.4.3 Some Issues for Improvement

The large signal characterization of the VI would provide better design procedures and options. This can be performed by taking the current and voltage waveforms for different values of reference current or by changing duty cycle manually, and then processing these data in *MATLAB* using system identification toolbox. From these analysis the large signal inductance value of the power inductor for each level of current (main current and control current if active) can be obtained and can be used get the large signal characterization of the power inductor prototype. This procedure was followed to characterize the power inductor for large signals, however, due to the parasitic effect

caused by the stacking of two cores, the voltage and current waveforms of the VI are affected by noise hence the expected results could not obtained.

Figure 26 presents two voltage waveforms to illustrate the parasitic effect oscillations. Besides, the large-signal characterization can be obtained from simulations in Finite Element Analysis softwares, it is going to be considered as one of the future plans of this work. Figure 26 (a) shows the voltage waveform when the duty cycle is 50% and Figure 26(b) shows the voltage for duty cycle of 52%. In both case considerable oscillations are noticed and this is mainly due to the prototype problem.

Furthermore, the global control layer is required to be automated. At the moment both current controllers are tested, but the dc-link controller is not tested. Due to availability limitation of dynamic electrical load, the dc-link controller is not tested. With better load the global control system can be verified. With the currently validated controllers, the control strategy based on the look up table obtained from set of experimental information is validated and provides superior performance. Nonetheless, the global closed loop control which includes the dc-link controller would provide much better results.

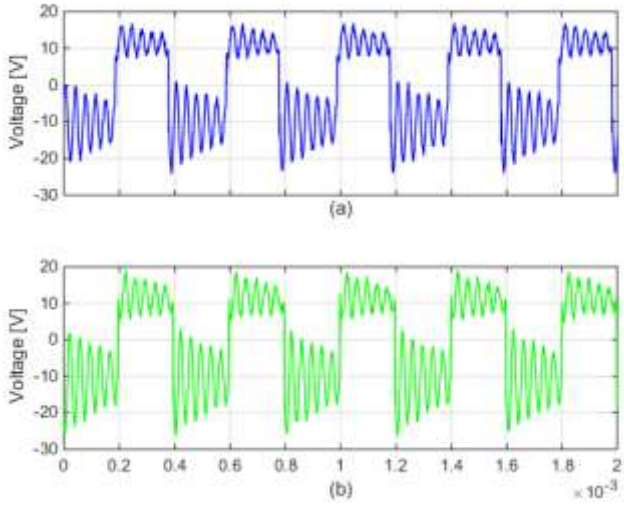

Figure 26: Voltage Waveforms (a) for D=0.5 (b) for D=0.52

One way to implement the control strategy is to sense the reference current in the main winding and compare it with the saturation level current. This limit can be a theoretical limit, obtained from the design procedure of the VI, or defined according to the actual behavior of the VI obtained with the large-signal experimental characterization. Then the

control winding controller can be initiated to provide regulated current to adjust the inductance so as to reduce the saturation effect or ripple according to the level of main winding current.

Another option is to measure the peak to peak value of ripple current and the average current of the main winding. Based on these measurements, the ripple percentage can be determined by dividing the peak to peak ripple to the average current and accordingly the control action can be taken when the ripple limit specification of the power inductor is exceeded. However, measuring the peak to peak current requires very fast microprocessors/DSP with high computing power.

CHAPTER 6 Conclusion and Future Works

6.1. Conclusions

This thesis presents the simulation and experimental validation of improved DC-DC converters for traction applications, special emphasis is given to the development of improved bidirectional DC-DC converter with VI. The bidirectional converter capability is achieved due the replacement of the conventional power inductor with a VI. The VI improved the performance of the bidirectional converter by providing better ripple control, which can lead to a power inductor with a reduced size and increasing saturation level of the power inductor.

The implemented VI is composed of two windings, where the control winding is used to adjust the main winding inductance in accordance of the current levels across the main winding in order to enhance the performance of the power inductor and the converter. The control winding is powered from a low-power buck converter. The control is realized as function of the main winding current in order to control the saturation level of the core and amount of current ripple.

The validity of the proposed VI and improved DC-DC converter are verified through experimental results. The implemented bidirectional converter with a VI and control converter provides superior performance in terms of ripple control, magnetic core saturation level improvement and increasing the current handling capability of power inductors. With the proposed scheme, the power inductor is capable of working at levels of current three times higher than the rated value with manageable current ripple.

Therefore, with the same core size the current handling capability is greatly improved, hence a remarkable step for core size optimization for power inductors. As the size of power converters is dominated by the power inductor, reducing the size and volume of power inductor will have significant reduction in the overall size of power converters for applications where space and weight are stringent requirements.

6.2. Future Works

This thesis has demonstrated the superior performance of half-bridge bidirectional DC-DC converter based on VI for sustainable transportation applications particularly focused in EV. The potential improvements in control of the current ripple during saturation of power inductors and the enhancement of the saturation level of power inductor for this specific application are verified with experimental procedures.

The concept of optimizing power converters with VI can be utilized in several areas such as renewable energy integration where there is unpredictable variation of resources and in applications where lighter weight of components is a stringent requirement (for instance in case of EV and flight electronics). Furthermore, this study is performed in half-bridge converter, it can be applicable in inverters and other DC-DC converters. This concept can also be further utilized for buffering of hybridized energy sources.

The thesis provides promising results in the optimization of power inductors and ripple control. However, there are several improvements and researches required to be addressed. First, to characterize the VI accurately and establish analytical procedures for designing and modeling of VI. Finite element analysis is very vital in order to fully understand the saturation behaviour of such power inductor under stress conditions (high demand of current levels, AC, DC or both).

In addition, the closed loop control of the global system and a control strategy to detect the saturation level of power inductors is very important to have an automated fast system. The closed loop control is implemented and the relationship between the two currents is obtained using curve fitting toolbox in *MATLAB.* Due to the availability limitation of dynamic electric loads, the dc-link control is not verified. With better sensors and load the global system will be tested and the concept will be verified fully.

This work revealed the promising significance of VI in power converter topologies improvement. For further improvements, it is necessary to have large signal characterization of power inductors and the characterization of power inductors as a function of both the main winding current and biasing winding current. With better cores

and high-speed microcontrollers the future task is to have a globally controlled system with better functionalities. In fact, new cores are obtained and the design and implementation of a new VI prototype is ready to be used for improving the performance and to repeat the tests to obtain better characterization of the VI concept. The long term plan of this work is to pursue it as part of my PhD research to continue improving the system for high power applications so that can be deployed in real systems to optimize the size of power converter topologies for sustainable transportation.

REFERENCES

[1] J. P. Trovão, P. G. Pereirinha, F. J. Ferreira, and H. M. Jorge, "Study of inductor effects in a bidirectional DC-DC converter for electrical vehicle," in Electrical Machines (ICEM), 2010 XIX International Conference on, 2010, pp. 1-6.

[2] S. S. Williamson, Energy Management Strategies for Electric and Plug-in Hybrid Electric Vehicles: Springer, 2013.

[3] J. Ivanovic, "Electric Vehicle Technology Explained," 2012.

[4] C. C. Chan and K. T. Chau, "An overview of power electronics in electric vehicles," Industrial Electronics, IEEE Transactions on, vol. 44, pp. 3-13, 1997.

[5] P. T. Krein, Elements of power electronics vol. 126: Oxford University Press New York, 1998.

[6] A. W. Lotfi and M. A. Wilkowski, "Issues and advances in high-frequency magnetics for switching power supplies," Proceedings of the IEEE, vol. 89, pp. 833-845, 2001.

[7] D. J. Perreault, H. Jingying, J. M. Rivas, H. Yehui, O. Leitermann, R. C. N. Pilawa-Podgurski, et al., "Opportunities and Challenges in Very High Frequency Power Conversion," in Applied Power Electronics Conference and Exposition, 2009. APEC 2009. Twenty-Fourth Annual IEEE, 2009, pp. 1-14.

[8] R. Lee, Electronic transformers and circuits: Reuben Lee, 1947.

[9] European Commission, "COMMUNICATION FROM THE COMMISSION TO THE EUROPEAN PARLIAMENT, THE COUNCIL, THE EUROPEAN ECONOMIC AND SOCIAL COMMITTEE AND THE COMMITTEE OF THE REGIONS " vol. COM(2013) 17 final p. 11, 24.1.2013.

[10] Communication on the Europe 2020 Flagship Initiative and Innovation Union, "Roadmap to a Single European Transport Area–Towards a competitive and resource efficient transport system," ed: White Paper, COM (2011), 2011.

[11] P. G. Pereirinha and J. P. Trovão, Multiple energy sources hybridization: the future of electric vehicles?: INTECH Open Access Publisher, 2012.

[12] Z. Dang and J. A. Abu Qahouq, "Evaluation of High Current Toroid Power Inductor with NdFeB Magnet for DC-DC Power Converters," Industrial Electronics, IEEE Transactions on, vol. PP, pp. 1-1, 2015.

[13] T. A. Burress, C. Coomer, S. Campbell, L. Seiber, L. D. Marlino, R. Staunton, et al., "Evaluation of the 2007 Toyota Camry Hybrid Syneregy Drive System," Oak Ridge National Laboratory (ORNL), Oak Ridge, TN2008.

[14] M. Tsili and S. Papathanassiou, "A review of grid code technical requirements for wind farms," IET Renewable Power Generation, vol. 3, pp. 308-332, 2009.

[15] F. Iov, A. D. Hansen, P. E. Sørensen, and N. A. Cutululis, Mapping of grid faults and grid codes: Risø National Laboratory, 2007.

[16] Y. A. Makandar and S. Vanamane, "Performance Analysis of Bidirectional DC-DC Converter for Electric Vehicle Application," International Journal for Innovative Research in Science and Technology, vol. 1, pp. 43-49, 2015.

[17] A. F. Restrepo, C. A. Ramos-Paja, and E. Franco, "Power Control of a Bidirectional dc Bus for Fuel Cells Applications," Revista EIA, pp. 159-170, 2012.

[18] M. Al Sakka, J. Van Mierlo, and H. Gualous, "DC/DC Converters for Electric Vehicles," Electric Vehicles–Modelling and Simulations, vol. 309, 2011.

[19] J. Zhang, "Bidirectional DC-DC power converter design optimization, modeling and control," 2008.

[20] K. Chau and Y. Wong, "Hybridization of energy sources in electric vehicles," Energy Conversion and Management, vol. 42, pp. 1059-1069, 2001.

[21] H. R. Karshenas, A. Bakhshai, A. Safaee, H. Daneshpajooh, and P. Jain, Bidirectional dc-dc converters for energy storage systems: INTECH Open Access Publisher, 2011.

[22] S. F. Tie and C. W. Tan, "A review of energy sources and energy management system in electric vehicles," Renewable and Sustainable Energy Reviews, vol. 20, pp. 82-102, 2013.

[23] D. M. Bellur and M. K. Kazimierczuk, "DC-DC converters for electric vehicle applications," in Electrical Insulation Conference and Electrical Manufacturing Expo, 2007, 2007, pp. 286-293.
[24] R. M. Schupbach and J. C. Balda, "Comparing DC-DC converters for power management in hybrid electric vehicles," in Electric Machines and Drives Conference, 2003. IEMDC'03. IEEE International, 2003, pp. 1369-1374.
[25] J. V. M. a. H. G. Monzer Al Sakka, "DC/DC Converters for Electric Vehicles, Electric Vehicles - Modelling and Simulations," (2011).
[26] M. Cacciato, F. Caricchi, F. Giuhlii, and E. Santini, "A critical evaluation and design of bi-directional DC/DC converters for super-capacitors interfacing in fuel cell applications," in Industry Applications Conference, 2004. 39th IAS Annual Meeting. Conference Record of the 2004 IEEE, 2004, pp. 1127-1133 vol.2.
[27] H.-J. Chiu and L.-W. Lin, "A bidirectional DC-DC converter for fuel cell electric vehicle driving system," Power Electronics, IEEE Transactions on, vol. 21, pp. 950-958, 2006.
[28] Z. Junhong, "Bidirectional DC-DC Power Converter Design Optimization, Modeling and Control," 2011.
[29] M. Marchesoni and C. Vacca, "New DC–DC converter for energy storage system interfacing in fuel cell hybrid electric vehicles," Power Electronics, IEEE Transactions on, vol. 22, pp. 301-308, 2007.
[30] F. Caricchi, F. Crescimbini, F. Giulii Capponi, and L. Solero, "Study of bi-directional buck-boost converter topologies for application in electrical vehicle motor drives," in Applied Power Electronics Conference and Exposition, 1998. APEC'98. Conference Proceedings 1998., Thirteenth Annual, 1998, pp. 287-293.
[31] F. Caricchi, F. Crescimbini, G. Noia, and D. Pirolo, "Experimental study of a bidirectional DC-DC converter for the DC link voltage control and the regenerative braking in PM motor drives devoted to electrical vehicles," in Applied Power Electronics Conference and Exposition, 1994. APEC'94. Conference Proceedings 1994., Ninth Annual, 1994, pp. 381-386.
[32] K. P. Yalamanchili and M. Ferdowsi, "Review of multiple input DC-DC converters for electric and hybrid vehicles," in Vehicle Power and Propulsion, 2005 IEEE Conference, 2005, pp. 160-163.
[33] O. Ichinokura, T. Jinzenji, and K. Tajima, "A new variable inductor for VAR compensation," Magnetics, IEEE Transactions on, vol. 29, pp. 3225-3227, 1993.
[34] A. Di Napoli, F. Crescimbini, L. Solero, F. Caricchi, and F. G. Capponi, "Multiple-input dc-dc power converter for power-flow management in hybrid vehicles," in Industry Applications Conference, 2002. 37th IAS Annual Meeting. Conference Record of the, 2002, pp. 1578-1585.
[35] A. Di Napoli, F. Crescimbini, S. Rodo, and L. Solero, "Multiple input DC-DC power converter for fuel-cell powered hybrid vehicles," in Power Electronics Specialists Conference, 2002. pesc 02. 2002 IEEE 33rd Annual, 2002, pp. 1685-1690.
[36] A. Di Napoli, F. Crescimbini, F. Guilii Capponi, and L. Solero, "Control strategy for multiple input DC-DC power converters devoted to hybrid vehicle propulsion systems," in Industrial Electronics, 2002. ISIE 2002. Proceedings of the 2002 IEEE International Symposium on, 2002, pp. 1036-1041.
[37] L. Zhu, "A novel soft-commutating isolated boost full-bridge ZVS-PWM DC–DC converter for bidirectional high power applications," Power Electronics, IEEE Transactions on, vol. 21, pp. 422-429, 2006.
[38] Y. Du, S. Lukic, B. Jacobson, and A. Huang, "Review of high power isolated bi-directional DC-DC converters for PHEV/EV DC charging infrastructure," in Energy Conversion Congress and Exposition (ECCE), 2011 IEEE, 2011, pp. 553-560.
[39] K. Yamamoto, E. Hiraki, T. Tanaka, M. Nakaoka, and T. Mishima, "Bidirectional DC-DC converter with full-bridge/push-pull circuit for automobile electric power systems," in Power Electronics Specialists Conference, 2006. PESC'06. 37th IEEE, 2006, pp. 1-5.
[40] A. Emadi, Y. J. Lee, and K. Rajashekara, "Power electronics and motor drives in electric, hybrid electric, and plug-in hybrid electric vehicles," Industrial Electronics, IEEE Transactions on, vol. 55, pp. 2237-2245, 2008.
[41] B. Arnet and L. Haines, "High power DC-to-DC converter for supercapacitors," in Electric Machines and Drives Conference, 2001. IEMDC 2001. IEEE International, 2001, pp. 985-990.

[42] O. Hegazy, R. Barrero, J. Van Mierlo, P. Lataire, N. Omar, and T. Coosemans, "An Advanced Power Electronics Interface for Electric Vehicles Applications," Power Electronics, IEEE Transactions on, vol. 28, pp. 5508-5521, 2013.
[43] O. Hegazy, J. Van Mierlo, and P. Lataire, "Control and analysis of an integrated bidirectional DC/AC and DC/DC converters for plug-in hybrid electric vehicle applications," Journal of Power Electronics, vol. 11, pp. 408-417, 2011.
[44] O. Hegazy, J. Van Mierlo, and P. Lataire, "Analysis, control and comparison of DC/DC boost converter topologies for fuel cell hybrid electric vehicle applications," in Power Electronics and Applications (EPE 2011), Proceedings of the 2011-14th European Conference on, 2011, pp. 1-10.
[45] O. Hegazy, J. Van Mierlo, and P. Lataire, "Analysis, Modeling, and Implementation of a Multidevice Interleaved DC/DC Converter for Fuel Cell Hybrid Electric Vehicles," Power Electronics, IEEE Transactions on, vol. 27, pp. 4445-4458, 2012.
[46] A. Perujo, G. Van Grootveld, and H. Scholz, Present and Future Role of Battery Electrical Vehicles in Private and Public Urban Transport: INTECH Open Access Publisher, 2012.
[47] M. Al Sakka, H. Gualous, J. Van Mierlo, and N. Omar, Batteries and supercapacitors for electric vehicles: INTECH Open Access Publisher, 2012.
[48] K. Chau, Y. Wong, and C. Chan, "An overview of energy sources for electric vehicles," Energy Conversion and Management, vol. 40, pp. 1021-1039, 1999.
[49] C. Chan and K. Chau, Modern electric vehicle technology vol. 47: Oxford University Press, 2001.
[50] R. de Castro, R. E. Araujo, J. P. F. Trovao, P. G. Pereirinha, P. Melo, and D. Freitas, "Robust DC-Link Control in EVs With Multiple Energy Storage Systems," Vehicular Technology, IEEE Transactions on, vol. 61, pp. 3553-3565, 2012.
[51] P. G. Pereirinha, J. P. Trovão, R. Castro, R. Araujo, P. Melo, D. Freitas, et al., Multiple energy sources hybridization: the future of electric vehicles?: INTECH Open Access Publisher, 2012.
[52] S. Dusmez, B. Bilgin, A. Khaligh, and M. Krishnamurthy, "A simple control scheme for active power filtering in ultracapacitor assisted plug-in hybrid electric vehicles," in Transportation Electrification Conference and Expo (ITEC), 2012 IEEE, 2012, pp. 1-6.
[53] M. S. Perdigao, J. P. F. Trovao, J. Alonso, and E. Saraiva, "Large-Signal Characterization of Power Inductors in EV Bidirectional DC–DC Converters Focused on Core Size Optimization," Industrial Electronics, IEEE Transactions on, vol. 62, pp. 3042-3051, 2015.
[54] Z. Dang and J. Abu Qahouq, "Evaluation of High Current Toroid Power Inductor with NdFeB Magnet for DC-DC Power Converters," 2015.
[55] S. Kimura, J. Imaoka, and M. Yamamoto, "Downsizing effects of integrated magnetic components in high power density DC-DC converters for EV and HEV," in Energy Conversion Congress and Exposition (ECCE), 2014 IEEE, 2014, pp. 5761-5768.
[56] M. Hirakawa, Y. Watanabe, M. Nagano, K. Andoh, S. Nakatomi, S. Hashino, et al., "High power dc/dc converter using extreme close-coupled inductors aimed for electric vehicles," in Power Electronics Conference (IPEC), 2010 International, 2010, pp. 2941-2948.
[57] S. M. Dwari and L. Parsa, "A novel high efficiency high power interleaved coupled-inductor boost DC-DC converter for hybrid and fuel cell electric vehicle," in Vehicle Power and Propulsion Conference, 2007. VPPC 2007. IEEE, 2007, pp. 399-404.
[58] L. Changrong and L. Jih-Sheng, "Low Frequency Current Ripple Reduction Technique with Active Control in a Fuel Cell Power System with Inverter Load," in Power Electronics Specialists Conference, 2005. PESC '05. IEEE 36th, 2005, pp. 2905-2911.
[59] M. Al Sakka, J. Van Mierlo, H. Gualous, and P. Lataire, "Comparison of 30KW DC/DC converter topologies interfaces for fuel cell in hybrid electric vehicle," in Power Electronics and Applications, 2009. EPE '09. 13th European Conference on, 2009, pp. 1-10.
[60] S. De Breucker, K. Engelen, R. D'Hulst, and J. Driesen, "Impact of current ripple on Li-ion battery ageing," in Electric Vehicle Symposium and Exhibition (EVS27), 2013 World, 2013, pp. 1-9.
[61] Z. Xi, Y. Chengliang, J. Ying, and P. Sanbo, "A Realtime APF Method for Battery Ripple Current Reduction in HESS-Based Electric Vehicles," in Vehicle Power and Propulsion Conference (VPPC), 2014 IEEE, 2014, pp. 1-5.
[62] L. Wujong, H. Byung-Moon, and C. Hanju, "Battery ripple current reduction in a three-phase interleaved dc-dc converter for 5kW battery charger," in Energy Conversion Congress and Exposition (ECCE), 2011 IEEE, 2011, pp. 3535-3540.

[63] Z. Junhong, L. Jih-Sheng, K. Rae-young, and Y. Wensong, "High-Power Density Design of a Soft-Switching High-Power Bidirectional dc–dc Converter," Power Electronics, IEEE Transactions on, vol. 22, pp. 1145-1153, 2007.
[64] W. Lee, B.-M. Han, and H. Cha, "Battery ripple current reduction in a three-phase interleaved dc-dc converter for 5kW battery charger," in Energy Conversion Congress and Exposition (ECCE), 2011 IEEE, 2011, pp. 3535-3540.
[65] H. Kosai, S. McNeal, B. Jordan, J. Scofield, B. Ray, and Z. Turgut, "Coupled inductor characterization for a high performance interleaved boost converter," Magnetics, IEEE Transactions on, vol. 45, pp. 4812-4815, 2009.
[66] D. S. Lymar, T. C. Neugebauer, and D. J. Perreault, "Coupled-magnetic filters with adaptive inductance cancellation," Power Electronics, IEEE Transactions on, vol. 21, pp. 1529-1540, 2006.
[67] L. Wuhua, X. Jianguo, W. Jiande, L. Jun, and H. Xiangning, "Application Summarization of Coupled Inductors in DC/DC Converters," in Applied Power Electronics Conference and Exposition, 2009. APEC 2009. Twenty-Fourth Annual IEEE, 2009, pp. 1487-1491.
[68] S. Zhou and G. A. Rincon-Mora, "A high efficiency, soft switching DC-DC converter with adaptive current-ripple control for portable applications," Circuits and Systems II: Express Briefs, IEEE Transactions on, vol. 53, pp. 319-323, 2006.
[69] C. N.-M. Ho, V. S. Cheung, and H. S.-H. Chung, "Constant-frequency hysteresis current control of grid-connected VSI without bandwidth control," Power Electronics, IEEE Transactions on, vol. 24, pp. 2484-2495, 2009.
[70] L. Corradini, P. Mattavelli, E. Tedeschi, and D. Trevisan, "High-Bandwidth Multisampled Digitally Controlled DC–DC Converters Using Ripple Compensation," Industrial Electronics, IEEE Transactions on, vol. 55, pp. 1501-1508, 2008.
[71] W. Rong-Jong and L. Chun-Yu, "Dual Active Low-Frequency Ripple Control for Clean-Energy Power-Conditioning Mechanism," Industrial Electronics, IEEE Transactions on, vol. 58, pp. 5172-5185, 2011.
[72] C. Ye-Then, Y. Chia-An, M. Hamaogi, F. Takahashi, and L. Yen-Shin, "Current ripple reduction technique of DC/DC converter," in Power Electronics, 2007. ICPE '07. 7th Internatonal Conference on, 2007, pp. 1087-1091.
[73] M. A. Al-Saffar and E. H. Ismail, "A high voltage ratio and low stress DC–DC converter with reduced input current ripple for fuel cell source," Renewable Energy, vol. 82, pp. 35-43, 2015.
[74] P. Cantillon-Murphy, T. C. Neugebauer, C. Brasca, and D. J. Perreault, "An active ripple filtering technique for improving common-mode inductor performance," Power Electronics Letters, IEEE, vol. 2, pp. 45-50, 2004.
[75] W. G. Hurley and W. H. Wölfle, Transformers and inductors for power electronics: theory, design and applications: John Wiley & Sons, 2013.
[76] T. C. Neugebauer, J. W. Phinney, and D. J. Perreault, "Filters and components with inductance cancellation," Industry Applications, IEEE Transactions on, vol. 40, pp. 483-491, 2004.
[77] E. S. Tez, "The parametric transformer," © Eyup Sali Tez, 1977.
[78] W. G. Hurley and W. H. Wölfle, Transformers and inductors for power electronics: theory, design and applications: John Wiley & Sons, 2013.
[79] Y. Bi and D. C. Jiles, "Finite element modeling of an electrically variable inductor," Magnetics, IEEE Transactions on, vol. 35, pp. 3517-3519, 1999.
[80] N. Benavides and P. Chapman, "Boost converter with a reconfigurable inductor," in Power Electronics Specialists Conference, 2007. PESC 2007. IEEE, 2007, pp. 1695-1700.
[81] L. Zhang, W. G. Hurley, and W. H. Wölfle, "A new approach to achieve maximum power point tracking for PV system with a variable inductor," Power Electronics, IEEE Transactions on, vol. 26, pp. 1031-1037, 2011.
[82] J. M. Alonso, M. A. Dalla Costa, M. Rico-Secades, J. Cardesin, and J. Garcia, "Investigation of a New Control Strategy for Electronic Ballasts Based on Variable Inductor," Industrial Electronics, IEEE Transactions on, vol. 55, pp. 3-10, 2008.
[83] H. Yuequan, L. Huber, Jovanovic, x, and M. M., "Single-Stage, Universal-Input AC/DC LED Driver With Current-Controlled Variable PFC Boost Inductor," Power Electronics, IEEE Transactions on, vol. 27, pp. 1579-1588, 2012.

[84] O. Ichinokura, T. Kagami, T. Jinzenji, M. Maeda, and Y. Wakiya, "High speed variable-inductor controlled with DC-DC converter," Magnetics, IEEE Transactions on, vol. 31, pp. 4247-4249, 1995.
[85] R. Hooper, B. Guy, and R. Perrault, "A current-controlled variable inductor," Instrumentation & Measurement Magazine, IEEE, vol. 14, pp. 39-44, 2011.
[86] J. M. Alonso, M. S. Perdigão, D. Gacio, L. Campa, and E. S. Saraiva, "Achieving constant frequency operation in DC-DC resonant converters through magnetic control," in Energy Conversion Congress and Exposition (ECCE), 2010 IEEE, 2010, pp. 2011-2018.
[87] M. Perdigao, J. Alonso, M. Dalla Costa, and E. Saraiva, "A variable inductor MATLAB/Simulink behavioral model for application in magnetically-controlled electronic ballasts," in Power Electronics, Electrical Drives, Automation and Motion, 2008. SPEEDAM 2008. International Symposium on, 2008, pp. 349-354.
[88] C.-Q. Lee, K. Siri, and A. K. Upadhyay, "Parallel resonant converter with zero voltage switching," ed: Google Patents, 1991.
[89] A. Kislovski, "Relative incremental permeability of soft ferrites as a function of the magnetic field H: an analytic approximation," in Power Electronics Specialists Conference, 1996. PESC'96 Record., 27th Annual IEEE, 1996, pp. 1469-1475.
[90] D. Medini and S. Ben-yaakov, "A current-controlled variable-inductor for high frequency resonant power circuits," in Applied Power Electronics Conference and Exposition, 1994. APEC'94. Conference Proceedings 1994., Ninth Annual, 1994, pp. 219-225.
[91] E. Rozanov and S. Ben-Yaakov, "Analysis of current-controlled inductors by new SPICE behavioral model," HAIT J. Sci. Eng. B, vol. 2, pp. 558-570, 2005.
[92] S. Ahsanuzzaman, T. McRae, M. M. Peretz, and A. Prodic, "Low-volume buck converter with adaptive inductor core biasing," in Applied Power Electronics Conference and Exposition (APEC), 2012 Twenty-Seventh Annual IEEE, 2012, pp. 335-339.
[93] MAGNETICS, "INDUCTOR DESIGN IN SWITCHING REGULATORS," Technical Bulletin, 2000.
[94] M. A. Swihart, "Inductor cores–material and shape choices," Magnetics®-www. mag-inc. com, 2004.
[95] C. W. T. McLyman, "Magnetic core selection for transformers and inductors," Energy, vol. 4, p. 4, 1997.
[96] D. M. Giuliano, M. E. D'Asaro, J. Zwart, and D. J. Perreault, "Miniaturized Low-Voltage Power Converters With Fast Dynamic Response," Emerging and Selected Topics in Power Electronics, IEEE Journal of, vol. 2, pp. 395-405, 2014.
[97] D. W. Hart, Power electronics: Tata McGraw-Hill Education, 2011.
[98] R. De Castro, J. P. Trovão, P. Pacheco, P. Melo, P. G. Pereirinha, and R. E. Araújo, "DC link control for multiple energy sources in electric vehicles," in Vehicle Power and Propulsion Conference (VPPC), 2011 IEEE, 2011, pp. 1-6.
[99] R. Kadri, J.-P. Gaubert, and G. Champenois, "An improved maximum power point tracking for photovoltaic grid-connected inverter based on voltage-oriented control," Industrial Electronics, IEEE Transactions on, vol. 58, pp. 66-75, 2011.
[100] A. V. Sant, V. Khadkikar, W. Xiao, H. Zeineldin, and A. Al-Hinai, "Adaptive control of grid connected photovoltaic inverter for maximum VA utilization," in Industrial Electronics Society, IECON 2013-39th Annual Conference of the IEEE, 2013, pp. 388-393.
[101] G. Terzulli, "Evolution of power capacitors for Electric Vehicles " p. 4.
[102] H. Wen, W. Xiao, X. Wen, and P. Armstrong, "Analysis and evaluation of DC-link capacitors for high-power-density electric vehicle drive systems," Vehicular Technology, IEEE Transactions on, vol. 61, pp. 2950-2964, 2012.
[103] M. A. Silva, J. P. Trovao, and P. G. Pereirinha, "Implementation of a multiple input DC-DC converter for Electric Vehicle power system," in Energetics (IYCE), Proceedings of the 2011 3rd International Youth Conference on, 2011, pp. 1-8.